Axon diversity of lamina I local-circuit neurons in the lumbar spinal cord

Journal:	*The Journal of Comparative Neurology*
Manuscript ID:	JCN-12-0308.R3
Wiley - Manuscript type:	Research Article
Keywords:	interneuron, propriospinal connection, varicosity distribution, propagation time, 3-D reconstruction

Axon diversity of lamina I local-circuit neurons in the lumbar spinal cord

Peter Szucs[1], Liliana L. Luz[1], Raquel Pinho[1], Paulo Aguiar[1,2], Zsófia Antal[3], Sheena Y.X. Tiong[4], Andrew J. Todd[4] and Boris V. Safronov[1]

1, Spinal Neuronal Networks Group, Institute of Molecular and Cell Biology - IBMC, University of Porto, Rua do Campo Alegre 823, 4150-180 Porto, Portugal; 2, Faculty of Sciences, Department of Applied Mathematics, Center of Mathematics of the University of Porto - CMUP, Porto, Portugal; 3, Department of Anatomy, Histology and Embryology, University of Debrecen, Medical and Health Science Centre, Nagyerdei krt. 98, 4032 Debrecen, Hungary; 4, Spinal Cord Group, College of Medical Veterinary and Life Sciences, University of Glasgow, University Avenue, G12 8QQ Glasgow, UK

Running head: Lamina I local-circuit neurons

Associate Editor: Gert Holstege / Brainstem and Spinal Cord Sensorimotor Systems

Key words: interneuron, propriospinal connection, varicosity distribution, propagation time, 3-D reconstruction

Corresponding author: Peter Szucs
Institute of Molecular and Cell Biology - IBMC, University of Porto
Rua do Campo Alegre 823, 4150-180 Porto, Portugal
e-mail: szucs@ibmc.up.pt
phone: +351-22-6074972
fax: +351-22-6099157

The work was supported by a grant from the Portuguese Foundation for Science and Technology funded by POCTI2010 and FEDER (B.V.S.) and the Wellcome Trust (A. J. T.). PSz and PA received financial support from FCT through the Ciência-2007 and POPH-QREN programs.

ABSTRACT (250)

Spinal lamina I is a key area for relaying and integrating information from nociceptive primary afferents with various other sources of inputs. While lamina I projection neurons have been intensively studied, much less attention has been given to local-circuit neurons (LCNs), which form the majority of the lamina I neuronal population. In this work the infrared light-emitting diode (IR-LED) oblique illumination technique was used to visualize and label LCNs, allowing reconstruction and analysis of their dendritic and extensive axonal trees.

We show that the majority of lamina I neurons with locally branching axons fall into the multipolar (with ventrally protruding dendrites) and flattened (dendrites limited to lamina I) somatodendritic categories. Analysis of their axons revealed that the initial myelinated part gives rise to several unmyelinated small-diameter branches that have a high number of densely packed large varicosities and an extensive rostrocaudal (2-3 segments), mediolateral and dorsoventral (reaching laminae III-IV) distribution. The extent of the axon and the occasional presence of long solitary branches suggest that LCNs may also form short and long propriospinal connections. We also found that the distribution of axon varicosities and terminal field locations show substantial heterogeneity and that a substantial portion of LCNs is inhibitory.

Our observations indicate that LCNs of lamina I form intersegmental as well as interlaminar connections and may govern large numbers of neurons, providing anatomical substrate for rostrocaudal "processing units" in the dorsal horn.

INTRODUCTION

Lamina I of the spinal cord is a key area for sensory information processing and pain transmission (Cervero and Tattersall, 1987; Christensen and Perl, 1970). It is a major target zone for the fine caliber myelinated Adelta- and unmyelinated C-primary afferent fibers (Willis and Coggeshall, 1991) as well as for the descending systems that control its activity (Millan, 2002). Based on their somatodendritic organization, lamina I neurons in the rat have been classified as fusiform (IA and IB), multipolar (IIA and IIB), flattened (III) and pyramidal (IV) (Lima and Coimbra, 1986). However, as for the rest of the dorsal horn and in particular of lamina I neurons, little is known about the local axonal projections and the lack of such information is a serious obstacle to establishing the roles of different neurons and understanding the dorsal horn circuitry (Todd, 2010). It is important to note that only 5% of lamina I neurons project supraspinally, while the majority of lamina I neurons function as excitatory and inhibitory intrinsic, or so-called local-circuit, spinal neurons (Cervero et al., 1979; Dickenson et al., 1997; Hunt et al., 1981; Bice and Beal, 1997; Grudt and Perl, 2002; Spike et al., 2003). Hence, lamina I neurons were shown to issue collaterals in laminae I-IV of the spinal cord in monkey (Beal et al., 1981), cat (Bennett et al., 1981; Hylden et al., 1986; Light et al., 1979) and rat (Cheunsuang and Morris, 2000; Grudt and Perl, 2002) as well as in the medullary dorsal horn of rats (Li et al., 2000). However, a systematic study on the functional connectivity of these neurons or the branching pattern and extent of their axons has not been performed yet. This is most likely due to the low yield of available techniques for labeling and reconstructing intact single neurons in lamina I.

The use of the IR-LED oblique illumination technique (Safronov et al., 2007; Szucs et al., 2009) in intact spinal cord preparations, in vitro, was proven to be a way to solve this problem. This approach permitted recording, labeling and reconstruction of the complete dendritic and axonal trees of lamina I neurons, revealing distinct local axon-collateral patterns for projection neurons belonging to the anterolateral tract (ALT) (Szucs et al., 2010). These experiments also revealed lamina I neurons with extensive local axons (see Fig.3. in Szucs et al., 2010) similar to those reported by Li et al. (2000) in the medullary dorsal horn. In a recent study we used a computer model of a 3-D reconstructed LCN to show that such complex axon architecture may significantly contribute to long

transmission delays in local monosynaptic connections (Luz et al., 2010). Thus, our aim in the present study was to provide a detailed morphological description of lamina I LCNs, with special emphasis on the axon structure, in order to improve our understanding of their role in the spinal dorsal horn network. We also aimed to create the first detailed 3-D reconstructions of lamina I neurons that besides being a valuable tool for computational neuroscience would also allow novel spatially dependent morphometric measurements.

MATERIALS AND METHODS

Spinal cord preparation

Laboratory Wistar rats (P14-P24) were killed in accordance with the national guidelines (Direcção Geral de Veterinária, Ministério da Agricultura) after anesthesia with intraperitoneal injection of Na^+-pentobarbital (30 mg/kg) and subsequent check for lack of pedal withdrawal reflexes. The vertebral column was quickly cut out and immersed in oxygenated artificial cerebrospinal fluid (ACSF) at room temperature. The lumbar spinal cord was dissected and the pia mater was locally removed in the region of interest with forceps and scissors to provide access for the recording pipettes. The spinal cord was glued with cyanoacrylate adhesive to a golden plate with the dorsolateral spinal cord surface facing upwards, and transferred to the recording chamber. All recordings were performed at 22-24 °C.

Segment length measurements

Lumbar spinal cords of P14 (n = 3) and P21 (n = 3) rats were excised as described above and immersion fixed in 4% paraformaldehyde to achieve a fixation that is comparable with that of the spinal cords used in electrophysiological experiments and for cell labeling. The rostrocaudal extent of the spread of rootlets from a given dorsal root was measured with a vernier caliper for all segments.

Imaging and identification of lamina I neurons

Lamina I neurons were visualized in the intact lumbar spinal cord using the oblique IR-LED illumination technique (Safronov et al., 2007; Szucs et al., 2009). Neurons were selected in the region between the dorsolateral funiculus (lateral border) and the dorsal root entry zone (medial border) (see Fig 1. in Pinto et al., 2010). The white matter covering this part of lamina I is thin in young rats, allowing visually-controlled tight-seal recordings from the superficial neurons. Neurons with multipolar or rounded somata were selected (Fig. 1A) since these somatic morphologies were unlike those of ALT-PNs described in our previous studies (Szucs et al., 2010; Luz et al., 2010). Only cells in the most superficial cell layer, with an apparent soma diameter above 20 μm were selected for recording.

Cell recording and filling

Recordings from lamina I neurons were made in whole-cell mode. The artificial cerebrospinal fluid (ACSF) contained (in mM): NaCl 115, KCl 3, $CaCl_2$ 2, $MgCl_2$ 1, NaH_2PO_4 1, $NaHCO_3$ 25, and glucose 11 (pH 7.4 when bubbled with 95%-5% mixture of O_2-CO_2). Pipettes were pulled from thick-walled glass (BioMedical Instruments, Germany) and fire-polished (resistance, 3-5 MΩ). The pipette solution contained (in mM): KCl 3, K-gluconate 150, $MgCl_2$ 1, BAPTA 1, HEPES 10 (pH 7.3 adjusted with KOH, final $[K^+]$ was 160 mM) and 0.5-1% biocytin. In the case of neurons that underwent further immunocytochemical analysis the 0.5% biocytin was complemented by 0.5% Rhodamine Red. Recordings were made with an EPC10-Double amplifier (HEKA, Lambrecht, Germany). The signal was low-pass filtered at 2.9 kHz and sampled at 10 kHz. Offset potentials were compensated before seal formation. Liquid junction potentials were calculated (15.9 mV) and corrected for in all experiments using the compensation circuitry of the amplifier. In some experiments substance P (SP; Sigma, St. Louis, MO) was applied in the bath through the perfusion line. Application of SP was never repeated in the same preparation.

Visualization of filled neurons and measurements

After fixation in 4% freshly depolymerized formaldehyde, the spinal cord was embedded in agar and 100 μm thick sagittal or transverse serial sections were prepared with a tissue slicer (Leica VT 1000S). To reveal biocytin, sections were permeabilized with 50% ethanol and treated according to the avidin-biotinylated horseradish peroxidase (HRP) method (ExtrAvidin-Peroxidase, diluted 1:1000;Sigma, St. Louis, MO) followed by a diaminobenzidine (DAB) chromogen reaction. Sections were either counterstained on slides with 1% toluidine blue, dehydrated, cleared and coverslipped with DPX (Fluka, Buchs, Switzerland), or treated with 1% OsO_4 and embedded in epoxy resin (Durcupan, Fluka, Buchs, Switzerland). Photomicrographs were taken using the 10x or 40x dry lens of a Primo Star (Zeiss) microscope equipped with a Guppy (Allied Vision Technologies) digital camera. In some cases multiple (3-6) photographs were taken from consecutive focal planes and overlaid in order to see focused details from different depths. These

photographs are referred to as extended focal images in the illustrations. Contrast and brightness of the photographic images used in all the figures were adjusted using the Adobe Image Ready software.

The area of filled neuronal somata were measured using the ImageTool software (University of Texas Health Science Center at San Antonio) by tracing the outline of the cell body with a mouse on digital images taken with a 10x objective lens.

In the case of 3-D reconstructed and connected cells, the largest extent of the axonal and dendritic tree in each direction was measured on the reconstructions. For cells that were not reconstructed and connected the measurements were performed on digital photographs or by overlaying a dimmed scale bar on the live image of the camera connected to the microscope. In sagittal sections the rostrocaudal extent could be directly measured and the mediolateral extent could be estimated by multiplying the number of sections that had labeled processes by the thickness of the sections. The dorsoventral extent in sagittal sections, especially in lateral ones, could not be measured reliably due to the curvature of the dorsal horn. In transverse sections, the mediolateral and dorsoventral extent could be directly measured while rostrocaudal extent was estimated in the same way as mediolateral extent for sagittal sections.

Due to the difficulty of the exact delineation of laminae in lateral sagittal sections laminar borders are not indicated on reconstructions from sagittal sections even when they are rotated to show a transverse view (e.g. Fig. 1E and F). Laminar location of axon branches was estimated by checking their distance from the dorsal surface (in medial sagittal sections where the dorsal horn curvature introduces less error) and from other landmarks, such as the notch at the level of the neck of the dorsal horn or the central canal. When these landmarks were located in more medial serial sections photographic images of the sections were overlaid for alignment.

3-D reconstruction

Complete 3-D reconstructions were performed from serial sections with Neurolucida (MBF Bioscience, Williston, VT). Since we found that the largest extent of the axonal tree of LCNs is in the rostrocaudal direction we chose cells sectioned in the sagittal plane

for reconstruction. This way there were fewer connections to be made between neighboring sections.

First, each section was completely traced into the corresponding section of a serial section dataset with a 40x (dry) objective. Caliber of the digitally traced processes was continuously adjusted during the tracing to completely cover the video image of the labeled process. Fiber caliber units for the selected lens were automatically set by the software, based on prior calibration. Whenever necessary, a 100x (oil immersion) lens was used to determine the Z difference between crossing structures. Neighboring sections were not aligned, nor were continuing processes connected at this point. Next, we aligned the sections and connected the pieces working always towards the section containing the soma. Due to shrinkage the thickness (Z-dimension) of resin embedded sections was 80-90% of the original 100 μm. This was comparable with shrinkage of these long sagittal spinal cord sections along the X-Y axes. Thus, Z-shrinkage was not corrected in these cases. In the case of DPX embedded material the shrinkage along the Z-axis was corrected to reach a thickness of 80 μm and to be comparable with the other reconstructions. In most cases, tracing and the procedure of alignment followed by connecting the corresponding pieces were performed by independent persons, to ensure that all difficult branch points and crossings were double checked. Section contours as well as gray matter and central canal borders were traced at the bottom level of each section. Neuronal processes that could not be connected due to partial filling, distortion of the sections or any other technical problems were deleted from the dataset. The estimated percentage of these deleted processes was below 5% in all cases.

Calculation and 3-D visualization of varicosity distributions and action potential propagation time maps

A set of specific functions (called Py3DN; https://sourceforge.net/projects/py3dn/) was developed in the Python programming language to perform particular, spatially dependent morphometric analyses on the axonal trees. The Neurolucida data of the reconstructed axon were made available to the Python environment using a custom made parser. The morphometric analysis algorithms were integrated into Blender, a well-

established free open source 3-D content creation suite (www.blender.org), to visualize the spatially dependent results.

For the visual representation of varicosity distribution along the axonal tree of LCNs, a virtual boundary box that encompasses the entire axonal tree was calculated. This volume was partitioned into voxels (or volume elements) with a predefined size (100 μm x 100 μm x 100 μm). The number of varicosities in each voxel was then calculated and its normalized value was used to color-code the particular voxel. For better visualization of the overlapping voxels, the opacity index of every voxel was also set to the normalized value of its varicosity content.

For creating propagation time maps along the LCN axonal trees, the time needed for a hypothetical action potential, initiated at the initial segment, to reach each point of the axon was calculated. The propagation time contribution of each axon segment (i.e. between two points of the reconstruction) was assumed to depend on its length and diameter. A diameter threshold based on electron microscopy measurements (see Fig. 7) was used to distinguish between myelinated and unmyelinated elements of the axon. The equation used for calculating the propagation time δ_m of myelinated regions was $\delta_m = l / (k_m d)$, where l is length, k_m is a constant factor and d is the diameter. The constant k_m was 10000 m/s·μm^{-1}, giving 10 m/s conduction velocity for a uniform 1-μm-thick constant diameter axon (Cervero et al., 1979). On the other hand, the equation used for calculating the propagation time δ_n for unmyelinated elements was $\delta_n = l / (k_n \sqrt{d})$, where l is the element length, k_n is a constant factor and d is the diameter. The constant k_n was chosen to be 380 m/s·μm$^{-1/2}$, which implies a conduction velocity of 0.38 m/s in a 1-μm-thick unmyelinated axon. This value was in good agreement with conduction velocities measured at 22-24 °C for unmyelinated C-fibers in isolated dorsal roots (Pinto et al., 2008). The cumulative propagation time for each axon point was calculated as the sum of propagation times of all elements up to the axon initial segment. A color code was used to represent the cumulative propagation time at each point of the axon. Due to the lack of data on the length of the axon initial segment of lamina I neurons, this part was treated as the rest of the axon tree.

Sholl analysis, path distance calculation and basic quantitative measurements were performed by Neuroexplorer (MBF Bioscience, Williston, VT).

Immunocytochemistry

Spinal cords containing neurons filled with a mixture of biocytin and rhodamine for immunocytochemistry were fixed in 4% formaldehyde for at least 24 hours at 4 °C. Serial sections of 60-100 μm thickness were prepared, in the sagittal or transverse plane, and a Zeiss AxioLab.A1 fluorescence microscope was used to identify the section containing the cell body. This section and its two immediate neighbors were treated with a cocktail of primary antibodies consisting of rabbit anti-vesicular GABA transporter (VGAT; 1:1000; Synaptic Systems, Goettingen, Germany) and guinea pig anti-vesicular glutamate transporter 2 (VGLUT2; 1:5000; Millipore, Watford, UK), as described previously (Yasaka et al., 2010). Filled cells were labeled with streptavidin-conjugated fluorochrome (avidin-rhodamine; 1:1000; Jackson ImmunoResearch, West Grove, PA) and species-specific secondary antibodies raised in donkey or goat and labeled with fluorescent dyes (Alexa 488, Pacific Blue, 1:500, Invitrogen, Paisley, UK; or DyLight 649, 1:100, Jackson ImmunoResearch) were used to perform triple fluorescence staining. Details of the antibodies are given in Table 1. The VGLUT2 antibody recognizes a band of 56 kDa (corresponding to the VGLUT2 protein) on Western blots of rat brain lysate. Its specificity was confirmed by carrying out dual immunofluorescence staining with a well-characterized rabbit antibody against VGLUT2 (Todd et al., 2003), and identical structures were stained by the two antibodies (Yasaka et al., 2010). The VGAT antibody stains a band of the appropriate molecular weight on Western blots (Guo et al., 2009). Immunofluorescence staining was blocked by pre-incubation with the immunizing peptide at 10^{-6}M (Polgar et al., 2011).

Sections were mounted, coverslipped with anti-fade medium and series of optical sections were acquired sequentially at 0.5 μm intervals with a Zeiss LSM 710 confocal microscope through a 63x oil-immersion lens (NA 1.4). Finally, sections were de-mounted and processed further with the HRP-DAB method for morphometric measurements or 3-D reconstruction (see above).

Electron microscopy

Spinal cords processed for electron microscopy analysis were fixed in a mixture of 4% formaldehyde and 0.1% glutaraldehyde. Serial sagittal 100-µm-thick sections were cut with a tissue slicer (Leica, VT 1000S). Sections were permeabilized by freeze-thaw cycles in liquid nitrogen and the biocytin revealed by the HRP-DAB reaction, as described above. Sections were postfixed in 1% OsO_4, dehydrated and embedded into epoxy resin (Durcupan, Fluka) on glass slides. Regions of interest were excised from the thin layer of resin on the slide and re-embedded for ultrathin sectioning. The ultrathin sections were further contrasted with lead-citrate (1 min) and uranyl-acetate (1 min), and scanned with an electron microscope (JEOL JEM 1400 TEM; Tokyo, Japan). Biocytin filled axonal profiles were digitally recorded using a Gatan SC 1000 ORIUS CCD camera (Warrendale, PA, USA) at 20000x or 50000x magnification. Diameter of axons and axon varicosities was measured on the digital images.

Numbers are given as mean ± SEM unless otherwise mentioned.

RESULTS

The following experiments aimed to characterize local-circuit neurons in the most superficial layer of the spinal dorsal horn. We have recorded from and filled 98 lamina I neurons, in the intact *in vitro* spinal cord preparation containing at least two- but in most cases all six (L1-L6) lumbar segments. In 82 cases the axon of the recorded neuron had been recovered to an extent that allowed us to confirm 1) the lack of any axon in the contralateral white or gray matter and 2) the presence of numerous ipsilateral, local axon collaterals with varicosities. These 82 neurons form the basis of this study.

The mean input resistance of LCNs was 0.9 ± 0.1 GΩ. With the exception of a few neurons, LCNs presented a tonic firing pattern and, in 46% of the cases, neurons were rhythmically firing action potentials (at zero injected current) that persisted in the presence of a blocker of fast glutamatergic transmission, CNQX (10 μM; Sigma, St. Louis, MO) (see Li and Baccei, 2011). About one-third of the LCNs tested (n = 34) responded with a characteristic inward current for the bath application of substance P (1 μM; Sigma, St. Louis, MO), an agonist of functional neurokinin-1 receptors. When recorded in current-clamp mode, the substance P-activated current caused depolarization that was often suprathreshold and resulted in sustained action potential firing. Analysis of the electrophysiological and pharmacological properties of LCNs will be the subject of another study.

From the 82 LCNs, 60 have been sectioned in the sagittal, 22 in the transverse plane and a total of 13 cells have been reconstructed. Complete 3-D reconstruction and connection of the reconstructed pieces was performed for 7 LCNs (cell IDs: L292_E1, L292_E5, L387_E3-2, L396_E2, L420_E2, Zs022_E8-1, L571_E20-3). For three more LCNs, 3-D reconstruction was performed (cell ID: Zs079_E13 – sagittal plane; cell ID: L315_E4 and L316_E6 - transverse plane) but connection of the pieces could not be performed due to distortion or damage to some of the sections. Three LCNs have been fully reconstructed and aligned in 2-D (cell IDs: L256_E1 and L279_E2 – sagittal plane; cell ID: L317_E1 – transverse plane) similarly to the reconstructions in Szucs et al. (2010). In addition, for comparison of basic parameters of the axon, a mixed-collateral-type (MCT) ALT-PN (cell ID: L292_E4) has also been reconstructed in 3-D.

Somatodendritic architecture of lamina I LCNs

Morphometric analysis of the somatodendritic domain was possible in 72 cases, where both soma and dendrites were revealed in detail. The majority of these recovered neurons fell into the multipolar (n = 38) and flattened (n = 29) somatodendritic types of Lima and Coimbra (1986). We also found 1 fusiform and 1 pyramidal-like soma in our sample while 3 neurons could not be classified according to this scheme. In the case of multipolar neurons (Fig. 1C, D and F), initial dendrites often originated close to each other resulting in a gradual tapering appearance of the soma towards the first dendritic branch point. Some of the multipolar dendrites protruded ventrally and reached lamina III (Fig. 1D and F and Fig. 2A and B), while dendrites of flattened neurons were mostly restricted to lamina I and outer lamina II (Fig. 1B and E). Dendrites of LCNs had few spines compared to those of ALT-PNs in our earlier study (see Fig. 1Db and Fig. 5A in Szucs et al., 2010).

LCNs had a mean soma diameter of 22.4 ± 0.6 μm (n = 72) and gave rise to 2-8 major dendrites (average: 4.4 ± 0.1). When comparing LCN soma areas and number of their initial dendrites with those of ALT-PNs from our previous study (n = 40; Szucs et al., 2010) we found that the majority of LCNs were smaller (average: 351 ± 17 μm^2) and gave rise to more initial dendrites than ALT-PNs (Fig. 1G). Basic morphometric parameters of the somatodendritic domain of LCNs are shown in Table 2. The rostrocaudal extent of the dendrites of LCNs was 320 ± 14 μm, while mediolateral and dorsoventral spread were 323 ± 15 μm and 159 ± 19 μm, respectively. Morphometric parameters of flattened and multipolar LCNs were similar. However, multipolar LCNs often gave rise to more dendrites and the dorsoventral extent of their dendrites, in line with the original description of lamina I multipolar neurons (Lima and Coimbra, 1986), was larger than that of flattened cells. The single fusiform and the pyramidal LCN along with the cells that could not be classified had larger dendritic trees. Sholl analysis of the branch-points (n = 7; reconstructed in 3-D) revealed that dendrites of LCNs branched mostly in the vicinity (50-250 μm) of the soma (Fig. 1H). We found no indication for any correlation between the somatodendritic type and investigated axon parameters of LCNs.

Axon of lamina I LCNs

The axon of LCNs in all cases formed a denser or sparser local network that spanned at least 1-2 segments rostrocaudally. Axon branches occupied the dorsal 100 - 120 micrometer-thick band of the grey matter (corresponding roughly to laminae I-II at this age), frequently protruded deeper, occasionally reaching the level of the notch at the neck of the dorsal horn (corresponding to laminae III-IV in most lumbar segments at this age and also in adult rats; Paxinos and Watson, 2007). Distribution of axon branches was also confirmed in transverse sections (Fig. 2A and C). In two cases a few axon collaterals reached below the level of the central canal (laminae VII and VIII). The local axon network was either centered on the soma (e.g. green neuron, cell ID: L292_E5, in Fig. 3A) or shifted along the rostrocaudal axis (e.g. red neuron, cell ID: L292_E1, in Fig. 3A or cell ID: L387_E3-2, in Fig. 6D). In most cases the axon overlapped with the dendrites and the soma. The mean rostrocaudal extent of the labeled and recovered axon of LCNs was 2312 ± 113 μm (Table 2) that corresponds to 2-3 lumbar spinal segments in animals at this age (Fig. 3B). Mediolateral and dorsoventral spread of the axon was 636 ± 27 μm and 295 ± 41 μm, respectively. While the extent of the axon of flattened and multipolar cells was similar in all dimensions, the axons of the other 5 neurons (fusiform, pyramidal and 3 not classified) were somewhat smaller (Table 2). The longest rostrocaudal extent encountered in this study was 6500 μm (red neuron, cell ID: L292_E1, in Fig. 3A). It has to be noted however, that in 51 of the 82 LCNs the axon reached one or both ends of the preparation and was therefore cut.

We used the neurons reconstructed in 3-D to compare total axon length, volume and branch points between LCNs and ALT-PNs. For the comparison, we used a characteristic, simple lateral-collateral type (LCT) ALT-PN from Luz et al. (2010) and additionally reconstructed a mixed-collateral type (MCT) ALT-PN that was filled along with two LCNs in the same spinal cord and, to date, has the most extensively branching ipsilateral collaterals in our ALT-PN sample (blue neuron, cell ID: L292_E4, in Fig. 3A). The filling time of the three neurons was almost identical: 28-30 minutes, although transport time of biocytin varied. The mean total axon length (i.e. sum of the length of all reconstructed axon segments) of LCNs was 32717 ± 4008 μm, which was comparable with the axon length of a complex MCT ALT-PN but a lot larger than that of the simple

LCT ALT-PN (Fig. 3C). The mean total axon volume (calculated from the length and diameter of all reconstructed axon segments) of LCNs was 2180 ± 378 μm^3, a value that falls between that of a complex MCT ALT-PN and the simple LCT ALT-PN (Fig. 3D). The mean number of branch points along the LCN axon was 247 ± 71, exceeding the value of even the most complex ALT-PN axon (Fig. 3E).

Occasionally, LCNs, situated in the most lateral part of lamina I, had the majority of their axon located medially, several tens of micrometers away from the soma (Fig. 4).
The main axon of LCNs originated from the soma (Fig. 5A) only in 36% of the cases, while the majority (46 of 82; 64%) branched from one of the primary dendrites (Fig. 5B) at a mean distance of 16.1 ± 1.6 μm from the soma (Table 3). The initial part of the axon had a myelinated appearance, similar to the main axon of ALT-PNs (Szucs et al., 2010), which persisted up to the first and second order, already thinner branches (Fig. 5C). In approximately half of the neurons this initial part of the axon made a ventro-dorsal and/or latero-medial loop, giving rise, often in an alternating manner (Fig. 5D), to 3-7 branches of smaller diameter that traveled rostrally or caudally and branched extensively. The overlapping axons of several branch orders formed the characteristic axon of LCNs (Fig. 5C). Axon branches started to have varicosities after 2-3 divisions. Initial divisions of the branches frequently occurred at acute angles (30-50 degrees), while distal branches, particularly the long rostrocaudal branches that run in the dorsolateral funiculus (DLF), gave rise to side branches in a perpendicular manner (Fig. 5E). The varicose part of the axon (i.e. most of the local axon in the vicinity of the soma) contained a great number of varicosities with a diameter between 0.5-1.5 μm (Fig. 5C). Apart from the local varicose axon network, 59 out of the 82 LCNs had single or multiple, varicose or myelinated looking solitary axon branches (Fig. 5F and G) in the neighboring white matter, including the Lissauer tract, dorsal funiculus (DF), DLF and lateral funiculus (LF). Detailed description of the locations and numbers of these axon branches is given in Table 3. The percentage of LCNs with axon branches in the neighboring white matter was highest (86%) among cells with flattened somatodendritic morphology and smallest (54%) in case of the 5 LCNs that were neither flattened nor multipolar. Axon branches in the white matter run both caudally and rostrally and we could establish neither a preferred direction

in our sample, nor any correlation with the location of the branches or any other descriptor of the neurons (e.g. somatodendritic type). None of the 82 LCNs in this study had detectable axon branches crossing the midline and entering the contralateral white matter.

Axon branching pattern

In order to understand how the intermingled axons of LCNs are organized we color-coded primary branches from the main axon of the 3-D reconstructed LCNs. In the sample of LCNs reconstructed in 3-D (n = 7), the maximum number of primary branches from the main axon was 7. We found overlaps between the target areas of the individual primary branches in all cases, despite the fact that they often started off in opposite directions in an alternating manner from the main axon (Fig. 6A and B). The overlap between target areas ranged from very slight (e.g. cell ID: Zs022_E8-1 in Fig. 6D) to substantial (Fig. 6C and also cell ID: L395_E2 in Fig. 6D). Some LCN axons had only 3-4 primary branches and the proximal ones (first or second) dominated the tree (Fig. 6A). In other LCNs, the major axon gave rise to up to 7 primary branches where distal ones occupied more space (Fig. 6C). In some cases proximal and distal primary branches targeted similar dorsal horn areas through separate routes and added further redundancy to the tree architecture (Fig. 6C).

Axon varicosity distribution

The axonal tree of LCNs possessed a large number (up to 6122, cell ID: L387_E3-2) of *en passant* varicosities and terminal boutons, typical for unmyelinated axons. The absolute number of detected varicosities in case of individual cells largely depends of the extent of labeling and the intactness of the axon, thus it is likely to show substantial heterogeneity. Varicosity density and distribution along the axon, however, may show characteristic patterns even in cases of incomplete cell labeling. Thus, we performed 3-D Sholl analysis and path distance measurements, combined with mapping of varicosity distribution along the axon in a spatially dependent manner. For the latter purpose, a custom made program was created that counted the varicosities in a predetermined space unit (voxel) and represented it visually on top of the 3-D representation of the axon. The

maximum varicosity number in the predefined voxels ranged from 79 to 273 among the 3-D reconstructed LCNs and the distribution along the axon was clearly heterogeneous (Fig. 7). As a general feature, all 6 neurons presented the highest number (and density) of varicosities in the vicinity (within the first 500 μm) of, but not centered on the soma (Fig. 7 and 8). The number and density of varicosities gradually decreased further away from the soma (e.g. cell IDs: L395_E2 and L387_E3-2, Fig. 7 and Fig. 8A). Path distance to the individual varicosities in these cells also showed a definite peak around 1000 μm. However, in cells that had fewer varicosities within the first 500 μm, we observed further local accumulation of varicosities that were sometimes located several hundreds of micrometers away from the soma along the rostrocaudal (e.g. cell IDs: Zs022_E8-1 and L292_E1, Fig. 7A and Fig. 8B) or mediolateral axes (e.g. L292_E5 in Fig. 7B). In these cells path distance histograms showed a more widespread distribution with multiple peaks (Fig. 8B).

One of the cells presented several such accumulations (cell ID: L292_E1, Fig. 7 and Fig. 8B) on side branches originating from a major projecting branch that run caudally for several segments, gradually becoming thinner. Interestingly, accumulations were spaced in a way that their position corresponded to different lumbar segments and while avoiding the region with dendrites of an MCT ALT-PN (cell ID: L292_E4, blue cell in Fig. 3), they overlapped with dendrites of another LCN (cell ID: L292_E5, green cell in Fig. 3).

Long solitary branches that projected out of the main part of the LCN axon usually had a constant diameter and were devoid of varicosities (consistent with the appearance of myelinated axons) except for occasional side bouquets (e.g. cell ID: L395_E2, Fig. 7).

Fine structure of LCN axons

Since the axon of LCNs could clearly be divided into varicosity bearing thin parts and thicker myelinated looking pieces, we wanted to confirm the absence and presence of myelin in these regions. Thus, we selected an LCN with a characteristic axon (Fig. 9A) and chose a section where myelinated looking thick pieces were present along with thin parts, densely packed with varicosities (Fig. 9B). The section was processed for electron microscopy analysis and two regions of interest (Fig. 9C and D - thick, myelinated

looking piece; Fig. 9E and F - thin varicose branches) were re-embedded and re-sectioned. We found that axonal profiles from the region shown in Fig. 9C and D, without exception, presented several concentric layers of myelin around them (Fig. 9G and H). At the same time, inter-varicosity segments (Fig. 9J) and varicosities (Fig. 9K) of axons from the region shown in Fig. 9E and F both lacked myelin.

We also measured the diameter of the axons on the electron microscopy photographs taken from the two regions of interest. Since the axons in the ultrathin sections were cut in a random orientation we first established the longitudinal axis of the particular profile and then measured the widest diameter perpendicular to it. Diameter histograms of myelinated (n = 24) and unmyelinated (n = 157) axon profiles are shown in Fig. 9I and in Fig. 9L. The mean diameter of myelinated axon profiles measured with- and without the myelin were 760 ± 28 nm and 453 ± 18 nm, respectively. Mean unmyelinated axon diameter was 311 ± 10 nm with most diameters in the bin between 200 and 250 nm. The ultrastructure of the preparation did not allow identification of further fine structural details or postsynaptic targets of the LCN axon.

Action potential propagation time in LCN axons

In an earlier study we estimated the action potential (AP) propagation times at different points of a complex LCN axon by using an anatomically correct neuronal model, where the whole axon was considered unmyelinated (see Fig. 8 in Luz et al., 2010; cell ID: L-395_E2). Our previous results indicated that the fine caliber and large length of LCN axons result in significant AP propagation times, up to tens of milliseconds. In the present study, however, our fine structural analysis revealed that some parts of the LCN axon are myelinated. Thus, we wanted to test to what extent the myelinated regions can reduce AP propagation time in the axonal tree. Furthermore, we wanted to calculate the theoretical AP propagation time for every point of the axonal tree to establish a temporal map of AP propagation in LCN axons. We developed a program in Python programming language to visually represent (in form of a color code) the propagation times (from 0 ms - blue, to the maximum value - red) for all points of the 3-D reconstructed LCN axons. The diameter threshold, above which we considered the axon segment as myelinated, has been set at 0.35 μm, based on the histograms and means of myelinated and unmyelinated

axon diameters (Fig. 9I and L). Conduction velocity in the unmyelinated part was set to 0.38 m/s for a uniform 1 μm thick axon in agreement with measurements done at 22-24 °C for unmyelinated C-fibers in isolated dorsal roots (Pinto et al., 2008). For myelinated axons we used a scaling factor giving a value of 10 m/s for a uniform 1 μm thick axon, so that the resulting conduction velocities fell in the range of those for the nociceptor-driven lamina I projection neuron axons of the small myelinated type (3.8-16.5 m/s; Cervero et al., 1979).

To create the AP propagation time maps we chose two LCNs (cell IDs: Zs022_E8-1 and L292_E1) with remotely situated terminal branching areas and also included, as a form of validation of the program, the LCN used in our earlier work (cell ID: L395_E2; Luz et al., 2010).

First we calculated conduction velocities for the axons considering them all as unmyelinated (Fig. 10A). The propagation times for cell L395_E2 were in the same range as those calculated using our former method (Luz et al., 2010). In the case of the LCN with the longest solitary branch (cell ID: L292_E1), the maximum propagation time in the remote regions was above 40 ms. In all 3 modeled LCNs the propagation time gradually increased in a concentric manner from the soma towards peripheral parts of the axon.

When propagation times were re-calculated considering axon segments with a diameter above 0.35 μm as myelinated, the maximum propagation times in each neuron dropped (Fig. 10B). For the LCN with a compact tree, lacking remote regions attached via thick long solitary branches (cell ID: L395_E2), the change in the maximum propagation time was negligible (about 2%, 23.9 ms changed to 23.5 ms). The propagation time distribution of the axon varicosities was only slightly shifted to the left with no apparent change in the shape (Fig. 10C).

For the other two neurons (cell IDs: Zs022_E8-1 and L292_E1), however, maximum propagation time dropped to around 80% of the original value (to 80.4% in case of Zs022_E8-1 and 83.7% in L292_E1). Changes in the propagation time map were most apparent in case of Zs022_E8-1 (see arrows on Fig. 10B). Propagation time distribution histograms of axon varicosities of the latter two LCNs were notably shifted to the left, and their temporal dispersion decreased (Fig. 10C).

Neurotransmitter content of LCN axon terminals

A question remaining after the description of the complex axon of LCNs was whether these neurons are excitatory or inhibitory. To answer this question, in 18 LCNs we tested immunoreactivity of the axon varicosities for antibodies raised against the vesicular GABA transporter (VGAT) and vesicular glutamate taransporter-2 (VGLUT-2) (Yasaka et al., 2010). In 16 LCNs, axon varicosities showed intensive immunolabeling for VGAT (Fig. 11A) and no sign of the presence of VGLUT-2 (not shown). In one LCN neither VGAT nor VGLUT-2 was detectable, while in another case the reaction was weak and immunopositivity could not be determined. To confirm that both transporters are indeed detectable in our preparation we tested their presence in dorsal, lateral and ventral collaterals of excitatory ALT-PNs (n = 4). Axon varicosities of the collaterals, as expected, proved to be VLGUT-2 immunopositive (images not shown). The mean soma area of the inhibitory LCNs, 246 ± 8 μm^2 (n = 6; somata recovered) was in the range of smaller cells in the LCN group (see Fig. 1G). Inhibitory LCNs belonged to the multipolar (n = 5) and flattened (n = 3) somatodendritic types (for cells where dendrites were recovered sufficiently for classification). The axon of the reconstructed inhibitory LCN (along with the rest of the analyzed inhibitory LCN axons) was similar to those of the rest of the LCN sample (Fig. 11B-E). This particular cell had an axon that showed accumulations of varicosities both on the caudal and rostral part of the tree (Fig. 11C).

DISCUSSION

We used the intact in vitro spinal cord preparation to demonstrate the axon diversity of LCNs in lamina I. We provided morphological evidence for their possible involvement in segmental interlaminar and propriospinal sensory information processing by showing that LCNs frequently possess a number of short and putative long propriospinal branches. To the best of our knowledge, for the first time, we provided extensive 3-D reconstructions of several lamina I neurons that allowed novel topological analyses. Besides the complexity of LCN axons, these analyses also revealed heterogeneity in the overlap between major axon branches, distribution of axon varicosities and in the estimated AP propagation times for different points of the axon.

Technical considerations

Our sample in this study is biased in some aspects. First, we used young animals, as the viability of the in vitro intact spinal cord preparation in our experiments proved to be best at P14-P24. For this reason, one cannot exclude that axons of more mature LCNs may be different. This, however, seems unlikely since lamina I neurons with very similar local axon branching pattern have been described in adult rats (Li et al., 2000). Second, due to the decreased visibility through regions rich in myelinated fibers, the medial part of the dorsal horn surface (dorsal root entry zone) was excluded from the search for neurons. Thus, conclusions of this study are based on neurons from the lateral two-thirds of lamina I. Third, when visualizing the surface of the dorsal horn in our intact spinal cord preparation, detection of the laminar border between lamina I and substantia gelatinosa relies solely on the appearance of the uniform, densely packed layer of small lamina II neurons. For this reason, to ensure that recorded neurons were in lamina I, we selected larger neurons in the most superficial (first to appear) cell layer of the dorsal horn. This way we unavoidably excluded small lamina I neurons. The description of axons of small lamina I and lamina II neurons will be the subject of another study.

Finally, full analysis of all investigated parameters was possible only in 3-D reconstructed neurons. However, the number of such reconstructions is relatively small compared to the total of the LCN sample resulting in an additional source of potential variance.

Somatodendritic architecture of LCNs

Based on their somatodendritic architecture, lamina I neurons in the rat have been classified into four categories: fusiform, pyramidal, flattened and multipolar (Lima and Coimbra, 1986). Lamina I LCNs in this study, with few exceptions, fell into the flattened and multipolar somatodendritic categories. This is in good agreement with our earlier study on local collaterals of lamina I ALT-PNs (Szucs et al., 2010) where none of the filled large multipolar neurons had an ascending axon in the contralateral anterolateral white matter.

Although lamina I neurons have the bulk of their dendritic arbors confined within this lamina (Gobel, 1978), we also showed in this study that multipolar neurons issue prominent ventrally protruding dendrites (Lima and Coimbra, 1986) that not only enter lamina II, as reported for human lamina I neurons (Schoenen, 1982) but also reach lamina III. Therefore, it is reasonable to assume that in addition to the common sources of input to lamina I neurons, multipolar cells integrate information from deeper laminae (e.g. from local axons and primary afferents terminating in laminae II and III) and should be treated as a separate group. Along this line, one cannot exclude the possibility that multipolar lamina I LCNs may even be activated monosynaptically by primary afferents that convey information to deeper laminae (e.g. A-beta afferents or A-delta hair follicle afferents; Todd, 2010). A detailed description of primary afferent input to lamina I LCNs, that may answer this question, is the subject of an ongoing study in our laboratory.

Similar to ALT-PNs (Szucs et al., 2010) a large percentage of LCN axons originated from one of the primary dendrites, although the mean distance from the soma in case of LCNs was slightly smaller. This, however, may be simply related to the fact that dendritic spread of LCNs was generally smaller than that of ALT-PNs reported in our previous study (Szucs et al., 2010). The high proportion of the axons with dendritic origin among LCNs suggests that this axon initiation type is a common feature of large lamina I neurons and is in agreement with earlier reports (Cheunsuang and Morris, 2000; Hylden et al., 1986). Dendritic origin of the main axon has also been observed in cat preganglionic sympathetic neurons (Morgan, 2001) and in motoneurons (Duflocq et al., 2011). This anatomical variation seems to be frequent in spinal cord neurons and

determining its functional importance will require further in-depth knowledge of the ultrastructure and ion-channel composition of the axon initial segment and the dendrites giving rise to them (Duflocq et al., 2011).

Overlaps between LCN axons and ipsilateral collaterals of lamina I ALT-PNs

While LCNs reported in this study all had collaterals located in the superficial dorsal laminae (I-II, occasionally entering III and IV), only about one third of ALT-PNs (32.5%; lateral and mixed collateral types) have ipsilateral collaterals in the same region (Szucs et al., 2010). This suggests that the influence of LCNs in laminae I-II is greater than that of the ALT-PNs. In the DLF the contribution to rostrocaudally oriented varicose axon collaterals from the two groups is more balanced: 39% of LCNs and 40% of ALT-PNs (lateral and mixed collateral types) have collaterals in this region. Thus, both types of lamina I neurons may relay local segmental information to neighboring segments and to neurons of the lateral spinal nucleus. Finally, information from lamina I to ventral laminae (V-VIII) is mostly relayed by collaterals of ventral- and mixed collateral type ALT-PNs (30%) as only a few LCNs (n = 2; 2.4%) had axons reaching lamina VII.

Possible roles of the local axon of LCNs

The extensive branching of LCN axons suggest that besides the anatomical divergence of primary afferent fibers, LCNs may provide further divergence of processed primary afferent information after integrating it with other sources of input. Furthermore, LCN axons occupy most dorsal laminae (I-II and occasionally III-IV) and this feature, theoretically, allows relaying of C-fiber information to deeper laminae. Indeed, Braz and Basbaum (2009) reported neurons in deep laminae (III-V) receiving polysynaptic input from unmyelinated primary afferents. Lamina I LCNs may be direct sources of such polysynaptic input or provide it through contacting lamina II islet and stalked neurons, that were shown to project to deeper laminae (Eckert et al., 2003). At the same time, multipolar LCNs may be monosynaptically activated by primary afferents that terminate in deeper laminae. Consequently, neurons in laminae III-V may integrate direct primary afferent information with indirect processed form of the same information through lamina I LCNs.

Due to their extensive local axon, relatively few LCNs could influence the superficial dorsal horn along several segments, in a sustained tonic manner based on their firing pattern and the frequent occurrence of rhythmic intrinsic firing.

The large number of varicosities and the highly branched, extensive axon of LCNs also imply that these neurons may be involved in volume transmission. In case of inhibitory LCNs, rhythmic intrinsic activity may result in continuous GABA release leading to metabotropic $GABA_B$ receptor activation in neurons of several neighboring segments.

While the majority of the tested LCN axons proved to be VGAT positive, for several reasons, it is likely that not all LCNs recorded in this study are inhibitory. Around 75% of neurons in lamina I of the rat spinal cord are neither GABA- nor glycine-immunoreactive, and these cells (many of which are LCNs) are thought to be glutamatergic (Polgár et al., 2003). Soma areas of inhibitory LCNs fell in the lower half of the total LCN soma area range, thus LCNs with larger somata may be the excitatory ones. Besides, in a previous study, we recorded synaptically connected lamina I neuron pairs, where the presynaptic neurons were always located in lamina I, and those connections were, without exception, excitatory (Luz et al., 2010). Furthermore, about one-third of the LCNs in this study expressed functional NK1 receptors (data not shown here), which were shown to be expressed in high percentage on lamina I projection neurons (Spike et al., 2003; Todd et al., 2000) and in excitatory interneurons (Littlewood et al., 1995), although the existence of NK1+/GABAergic neurons has also been proposed in the spinal (Ferrini at el., 2007) and in the medullary (Wang et al., 2000) dorsal horn of rats.

We demonstrated that while the general appearance of the complex local axon is similar in all LCNs, axon varicosity distribution and branching pattern show certain heterogeneity. This may be related to the segmental position or to the location of a particular LCN in the somatotopic map. The relatively low number of 3-D reconstructed axons that could be used for such topological analyses, however, did not allow us to establish such correlations.

Functional consequences of the organization of LCN axons - branching, varicosity distribution and spike propagation

The complex axon of LCNs with large numbers of varicosities, a tonic firing pattern, together with the observation that some of these neurons are rhythmically active (data not shown here), suggest that LCNs could provide tonic regulation and could distribute integrated information in a pattern governed by inherent spatial and temporal properties of the axon.

For a complex axon with thousands of varicosities, forming networks in a highly somatotopic spinal dorsal horn, temporal dispersion of synaptic output is of crucial functional importance. The propagation time of an AP, initiated in the axon initial segment, is mostly determined by path length, axon diameter, myelination and branching (Debanne et al., 2011). Path distance to a particular point of the axon is strongly dependent on branching. The alternating branching of primary collaterals from the main axon into the rostral and caudal directions, frequently observed in this study, seems to be an efficient solution for maximally filling the target space (laminae I-III) and, at the same time, equalizing path distance for the rostral and caudal portions of the axon tree. This set up, however, in a system with strong spatial boundaries, such as the spinal dorsal horn, results in an overlap between major branches. Target regions supplied by multiple overlapping branches may be activated repeatedly, thus it will be important to understand conduction properties of LCN axons to evaluate their role in the spinal network.

A recent paper comparing 3-D reconstructed basket and spiny cell axons used uniform conduction velocities to estimate, among other things, temporal dispersion in the axonal trees (Budd et al., 2010). The authors pointed out that this approach might underestimate temporal economy as, for example, myelinated primary axon collaterals could reduce latency to child branches with the same amount of axon for wiring. Myelinated long range branches of GABAergic interneurons, running in the stratum moleculare between innervation regions have been shown recently in the hippocampus (Jinno et al., 2007). In this paper we also demonstrated the presence of myelin around thicker initial parts of the axon of LCNs and, indeed, when we used a diameter-threshold to distinguish myelinated parts of LCN axons, temporal dispersion of AP propagation in

the tree was reduced. This effect seemed to be more prominent in cells with remote varicosity fields connected by thicker, probably myelinated, axon pieces.

Although in our simulation of AP propagation in the complex axon of LCNs we considered the presence of myelin, this is still a simplified approach. Unfortunately, experimental data on other important factors (e.g. voltage-gated ion channel types and densities), with the exception of some parts of substantia gelatinosa neuron axons (Safronov et al., 1997; Safronov, 1999), are not available for different parts of the axons of spinal neurons. The diameter threshold for myelinated axons (0.35 μm) was chosen from measurements in a single neuron but it is in agreement with the diameter reported for unmyelinated cortical axons (0.08-0.4 μm, Westrum and Blackstad, 1962; Berbel and Innocenti, 1988). It also has to be noted that our simulated AP propagation times in LCN axons are probably overestimations, since the constants used for calculating non-myelinated segment conduction velocities are based on measurements done at room temperature. In a living organism the AP propagation times must, therefore, be shorter. Our goal, however, was to prove that the adequately positioned myelinated regions of the axon significantly alter the AP propagation times in remote parts of the axon tree.

APs traveling through several sudden diameter irregularities such as axon varicosities were suggested to suffer additional delay (Manor et al., 1991), while passing through several branch points may even result in a failure of propagation (Debanne et al., 1997). In the case of LCNs with thousands of varicosities this could mean significant further increase in propagation times and may even cut off some parts of the axon tree from signal invasion temporarily.

Subthreshold signal propagation within LCN axons could also lead to robust functional differences in different parts of the tree. Recent direct recordings from axonal structures in the hippocampus and neocortex suggested that subthreshold graded signals propagate down the axon over distances of up to 1 mm. At certain synapses, these analog axonal signals were shown to modulate AP-dependent transmitter release (Alle and Geiger, 2008). The same mechanism in LCN axons could modulate synaptic output at varicosities in the vicinity of the cell body as opposed to remote varicosities. For example, the SP-induced depolarization observed in almost half of the LCNs (data not shown here) could also propagate down the LCN axon and may boost transmitter release.

Given the complexity of LCN axons and their accessibility due to their superficial location, they could be ideal targets for studies on axon conduction by using novel imaging techniques, such as high-speed fluorescent sodium imaging with high temporal and spatial resolution (Fleidervish et al., 2010; Foust et al., 2010), *in vitro* or *in vivo*.

Long propriospinal connections of lamina I LCNs

While LCNs clearly do not project through the lateral funiculus on the contralateral side, for several reasons, it seems likely that they may also function as short and long propriospinal neurons.

As we report here, a large percentage of LCNs (86% of flattened and 69% of multipolar neurons) had long solitary axon branches, often with myelinated appearance, in the DF, DLF and in Lissauer's tract. These branches had no preferential direction and often run 2-3 segments in the rostral or caudal direction before fading below visibility and were similar to those described in earlier anatomical studies (Lenhossek, 1895; Cajal, 1905; Szentagothai, 1964).

The presence of such collaterals is also in line with electrophysiological observations. About one third of nociceptor driven lamina I neurons could be antidromically activated by stimulation of Lissauer's or deeper tracts from up to 3 segments rostral to their origin (Cervero et al., 1979). The conduction velocity of the axons of these neurons suggested that they are small and myelinated (Cervero et al., 1979). In addition unmyelinated propriospinal axons were also observed in the DLF at the sacral level (Chung et al., 1988). These latter fibers, as we showed earlier (Szucs et al., 2010) and also in this paper (see blue neuron, cell ID: L292_E4, in Fig. 3), could also include lateral collaterals of ALT-PNs. Taking all this together it is reasonable to say that a substantial proportion of axons in the DLF are indeed propriospinal fibers and form massive intersegmental connections. These connections are not only formed by axons of lamina II-III neurons resulting in a closed system (Szentagothai, 1964), but also by collaterals of lamina I neurons, some of which serve as major output elements of the dorsal horn circuitry.

Lenhossek (1895), Cajal (1909) and Szentagothai (1964) described lamina II-III neurons with several segment-spanning, rostrocaudally oriented axons in Lissauer's tract

and intersegmental integration was also proposed recently for dorsal horn cholinergic neurons, with similar rostrocaudal axonal organization (Mesnage et al., 2011). However, some LCNs in our study possess morphological features that would also allow them to establish not only short but also long propriospinal connections. Solitary branches in the DF, DLF and Lissauer's tract never crossed the midline and run rostrally until they faded or reached the end of the spinal cord block, providing anatomical substrate for such long propriospinal projections. Indeed, previous reports suggested that around one quarter of lamina I neurons have long ascending propriospinal projections that extend from the lumbar to at least mid-thoracic spinal levels, but do not reach the brain (Bice and Beal, 1997a,b) Thus, the long solitary branches, observed in some of our LCNs, may be long propriospinal branches indicating that at least some LCNs may have influence on distal spinal cord regions. To test this hypothesis further careful morphometric analysis of LCN axons will be needed combined with retrograde labeling from distal spinal cord segments. Eventually, understanding of local connections and outputs of lamina I neurons will allow designing better strategies for intercepting pain signals at the spinal cord level.

FIGURE LEGENDS

Figure 1. Somatodendritic features of LCNs. **A:** Images of large (left pair) and smaller (right pair) LCNs during the process of cell labeling. **B:** Photomicrograph of the soma, dendrites and axon branches of a typical flattened LCN in a sagittal spinal cord section. **C:** Photomicrograph of a typical multipolar LCN in a sagittal section. **D:** Another multipolar LCN in a transverse section. Dashed white line indicates the rough borders of lamina II. The section is slightly distorted due to detachment from the supporting agar during processing. **E:** Sagittal (left) and transverse (right) rotated views of a 3-D reconstructed flattened LCN (reconstruction from sagittal sections; axon omitted for clarity). **F:** Sagittal (left) and transverse (right) rotated views of a 3-D reconstructed multipolar LCN (reconstruction from sagittal sections; axon omitted for clarity). **G:** Histograms of soma area distribution (left) and number of stem dendrites (right) in LCNs (gray bars) and ALT-PNs (outlined empty bars). The data for the ALT-PNs are from Szucs et al. (2010). **H:** 3-D Sholl analysis of the number of dendritic branch points in 50-μm-thick shells. C, caudal; M, medial; D, dorsal; R, rostral (throughout the figures). Binsizes in G = 50 μm^2 in the soma area histogram; 1 in the stem dendrite histogram. Scale bars = 20 μm in A; 50 μm in B-D.

Figure 2. A typical multipolar LCN reconstructed from transverse serial sections. **A:** Overlaid image of 15 transverse, 100 μm thick, serial sections. Dendrites (black) and axon (dark gray) of the LCN (cell ID: L316_E6) occupy laminae I-II and protrude into lamina III. An axon collateral descends ventrally beyond the neck of the dorsal horn, while some dendrites are located in the DLF. For clarity, borders of the white and gray matter (continuous light gray line; same in B and C) as well as of lamina II (dashed light gray line; same in B and C) are only shown for the section containing the cell body. **B:** Reconstructions showing the location of dendritic pieces (black) in the individual transverse serial sections. **C:** Reconstructions indicating the location of axonal pieces (black) in the individual transverse serial sections. soma, section with the cell body; r, rostral; c, caudal. Scale bar = 500 μm.

Figure 3. Comparison of basic axon parameters of 3-D reconstructed LCNs and ALT-PNs. **A:** 3-D reconstruction of two LCNs (cell ID: L292_E1 - in red; cell ID: L292_E5 - in green) and a mixed-collateral-type (MCT) ALT-PN (cell ID: L292_E4 - in blue), filled in the same spinal cord. Rostrocaudal, mediolateral and dorsoventral dimensions of the bounding box (light gray) are indicated along the corresponding axis. **B:** Length of different lumbar spinal cord segments (L1-L6) at postnatal days 14 (P14) and 21 (P21). Columns in each case show the average and standard mean error of measurements in 3 different animals. **C-E:** Total axon length (i.e. sum of the lengths of all reconstructed axon segments), total axon volume (i.e. sum of all reconstructed axon segment volumes, calculated from segment length and local diameter) and number of branch points along the axon of individual cells (red, green, blue and white outline columns) along with the mean value for 3-D reconstructed LCNs (gray column; n = 7).

Figure 4. Sagittal (**A**), horizontal (**B**), transverse (**C**) and perspective (**D**) view of a 3-D reconstructed but not fully connected LCN (cell ID: Zs079_E13). The majority of the axon (yellow) in this case is located medially, considerably remote from the lateral cell body and dendrites (orange). The neuron has a solitary branch running caudally in the dorsolateral funiculus on the ipsilateral side. The medial part of the axonal tree, due to distortion of some sections, could not be connected to form a single axon. White and gray matter borders are indicated with gray and central canal is shown in green. Scale bar = 1 mm.

Figure 5. General morphological features of the axon of LCNs. Main axon (asterisk) originating from the soma **(A)** and from a primary dendrite (**B**) of two LCNs. Arrows point at the axon origin. **C:** Characteristic appearance of LCN axons in the vicinity of the cell body. The main axon (asterisk) along with primary and secondary order branches (arrowheads) are intermingled with fine terminal branches enriched with varicosities (t). **D:** The main axon (asterisk) of an LCN giving rise to primary branches (arrowheads) in an alternating manner. **E:** Perpendicular side branch from a solitary axon branch running in the dorsolateral funiculus. **F:** Straight thick solitary axon with swellings together with a more undulated thin varicose also solitary branch next to the surface of the preparation,

most likely in the Lissauer tract. **G:** Thick, myelinated looking solitary branch of an LCN, running in the dorsal funiculus. A-E, G - extended focal images; F - single focal plane image. Scale bars = 25 μm.

Figure 6. Organization of the primary axon branches of LCNs. **A:** Sagittal (top), transverse (middle left) and horizontal (bottom) view of the 3-D reconstruction of an LCN with 5 primary branches (cell ID: L420_E2) where the first and second branches (orange and yellow) dominate the tree showing partial overlap with the rest of the branches. The end of the main axon turns caudally and finishes abruptly close to the surface; most likely damaged when pia mater was removed during preparation. **B**: Main axon and the origination points of each primary branch. Note the dorsoventral loop of the main axon. **C:** Another LCN (cell ID: L292_E5) with 7 primary branches, from which the last two (light blue and dark blue) covers the largest area. Similarly to the previous cell, the main axon forms a loop before it finishes abruptly close to the surface with a visible swelling at the end, probably caused by truncation. The first primary branch (orange) of this axon traverses the dorsal horn medially and target similar regions than the last branch (dark blue). **D**: Sagittal view of 3-D reconstructions of 4 other LCNs. Cell IDs are indicated on the left side of the corresponding reconstruction. Colored boxes in the bottom of the figure indicate the color codes of the sequence of primary axon branches. S/d, soma and dendrites; main, main axon; 1st-7th, the respective order of primary branches from the main axon. Scale bars = 500μm in A and C; 1 mm in D.

Figure 7. Varicosity distribution along the axon of LCNs. Spatially dependent visual representation of axon varicosity distribution from sagittal (**A**) and horizontal (**B**) views, as indicated on the schematic drawings above each column. Axon varicosities along the 3-D reconstructed LCN axons were counted in predetermined space units (voxel). The maximum varicosity number in the predefined voxels (100 μm x 100 μm x 100 μm) is indicated as the maximum value (red) on the scale bar next to the particular neuron. The actual number of varicosities in a voxel is used as a color and opacity value for the cube representing that voxel. Cell IDs are indicated on the left side of the figure. 3-D scale bars (D, dorsal - green; L, lateral - blue; R, rostral - red) = 250 μm.

Figure 8. Physical and path distance of axon varicosities in 3-D reconstructed LCN axons. Sholl analysis was performed using 100 μm shells. Binsize in path distance histograms is 100 μm. **A:** Three cells showing a major accumulation of varicosities in the vicinity of, but not centered on the soma, with one peak both in the Sholl analysis and in the path distance histogram. **B:** Other LCNs, with lower overall number of varicosities, showed additional local accumulations, evidenced by multiple peaks in the Sholl analysis, and at the same time wider distribution of the path distance histogram. Notice the different scaling of the Y-axis between **A** and **B** and also the difference on the X-axis in cell ID: L292_E1 in part **B**.

Figure 9. Fine structural difference between myelinated and unmyelinated parts of an LCN axon. **A:** 2-D reconstruction of a representative LCN axon (cell ID: L279_E2). **B:** 2-D reconstruction of a single section of the same axon. Light gray processes are dendrites (d) while axon is in black. Continuous and dotted gray lines indicate the border of the section and border between the gray- and white matter, respectively. Boxes indicate regions of interest with a single myelinated looking axon branch (C-D) and several varicose branches (E-F). **C-F:** show the reconstruction of the corresponding region and a photomicrograph of the same region from the surface of the block used for preparing the electron microscopy sections. Black parts of the reconstructions in C and E show axon pieces still present on the block surface, while gray indicate parts that were already cut. **G-H:** Electron microscopic images of axon profiles from region C-D with several concentric layers of myelin. **I:** Diameter histogram of axon profiles (n = 24) from the same region measured with (outlined hollow bars) and without myelin (gray bars). **J:** Electron microscopic image of an inter-varicosity segment and a varicosity (**K**) from region E-F. **L:** Diameter histogram of axon profiles (n = 157) from the same region. Bins = 50 nm in I and L. Scale bars = 1 mm in A; 50 μm in B; 10 μm in C, D, E and F; 500 nm in G, H, J and K.

Figure 10. Action potential propagation time maps of LCN axons. **A:** Sagittal view (see schematic figure in upper right) of a cell (ID: L395_E2) with a more compact tree and

two cells (IDs: Zs022_E8-1 and L292_E1) with distant terminal branching areas. The whole axon is considered unmyelinated. **B:** AP propagation time maps of two cells (IDs: Zs022_E8-1 and L292_E1) re-plotted assuming that axon pieces with a diameter above 0.35 μm are myelinated. The maximum propagation time value in the map is indicated by red, while 0 ms is blue on the scale bar next to the particular neuron. Arrows point at regions where the propagation time map shows visible differences. **C:** Propagation time histogram of the axon varicosities of the three LCNs shown in A. Bins = 1 ms. Gray bars, total axon unmyelinated; red outlined transparent bars, axon pieces with a diameter above 0.35 μm are myelinated.

Figure 11. Example of an inhibitory LCN**. A:** Single section of a biocytin filled axon (magenta) of an LCN (cell ID: L571_E20-3). Arrows with numbers indicate the VGAT immunoreactive axon varicosities (green) shown in detail in the insets on the right side. Small arrows in the inset point at the actual varicosity. The main image is projected from 36 optical sections at 0.5 μm z-spacing, while images in the insets are single optical sections. **B:** Primary branch organization of the same LCN axon shows relatively few overlap between the branches. **C-D:** The number of axon varicosities in this axon is moderate and varicosity distribution show more than one, relatively dispersed accumulations. **E:** Temporal dispersion of action potential propagation times in the same LCN axon did not show noticeable difference when using the diameter threshold for myelinated axons, indicating the lack of long myelinated parts in the axon. Scale bars = 10 μm in A; 5 μm in insets. Bins = 100 μm in D; 1 ms in E.

Table 1. Details of the Antibodies Used.
VGLUT2, vesicular glutamate transporter 2; VGAT, vesicular GABA transporter; KLH, keyhole limpet haemocyanin.

Table 2. Basic Morphometric Parameters of the Somatodendritic and Axonal Domains of LCNs.[1]
[1]Data are presented as mean ± SEM and the range (in brackets). [2]Neurons where the soma was not recovered (n = 10) were excluded from the analysis of the dendritic tree.

SD type, somatodendritic type determined using criteria of Lima and Coimbra (1986); n.c., not classified; n.a., not applicable for neurons where the soma was not recovered; stem, number of stem dendrites from the soma; RC, rostrocaudal; ML, mediolateral; DV, dorsoventral; cut, the axon of the cell reached one or both ends of the spinal cord preparation and, consequently, was severed; plane, sectioning plane; S, sagittal; T, transverse.

Table 3. Morphological Description of the Axon of LCNs.[1]

[1]Data are presented as mean ± SEM and the range or percentage (in brackets). [2]Neurons where the soma was not recovered (n = 10) were excluded from the analysis of the dendritic origin of the axon. SD type, somatodendritic type determined using criteria of Lima and Coimbra (1986); n.c., not classified; n.a., not applicable for neurons whose soma was not recovered; distance, distance from soma to the axon origin point along the dendrite; GM, gray matter; WM, white matter; DF, dorsal funiculus; DLF, dorsolateral funiculus; LF, lateral funiculus; ipsi-, ipsilateral; contra-, contralateral; ALT, anterolateral tract.

OTHER ACKNOWLEDGMENTS

The authors would like to thank Dr. Zita Puskár and Prof. Deolinda Lima for their constructive comments and Rui Fernandes for his technical help with electron microscopy.

CONFLICT OF INTEREST STATEMENT

None of the authors have any conflicts of interest.

ROLE OF AUTHORS

All authors had full access to all the data in the study and take responsibility for the integrity of the data and the accuracy of the data analysis.

Study concept and design: PSz, PA, AT

Acquisition of data: LLL, PSz, RP, SYXT, AT, ZsA

Analysis and interpretation of data: PSz, PA, SYXT, AT

Drafting of the manuscript: PSz

Critical revision of the manuscript for important intellectual content: PSz, BVS, AT, PA

Obtained funding: BVS, AT

Study supervision: PSz

Literature cited

Alle H, Geiger JR. 2008. Analog signalling in mammalian cortical axons. Curr Opin Neurobiol 18(3):314-320.

Beal JA, Penny JE, Bicknell HR. 1981. Structural diversity of marginal (lamina I) neurons in the adult monkey (Macaca mulatta) lumbosacral spinal cord: a golgi study. J Comp Neurol 202(2):237-254.

Bennett GJ, Abdelmoumene M, Hayashi H, Hoffert MJ, Dubner R. 1981. Spinal cord layer I neurons with axon collaterals that generate local arbors. Brain Res 209(2):421-426.

Berbel P, Innocenti GM. 1988. The development of the corpus callosum in cats: a light- and electron-microscopic study. J Comp Neurol 276(1):132-156.

Bice TN, Beal JA. 1997. Quantitative and neurogenic analysis of neurons with supraspinal projections in the superficial dorsal horn of the rat lumbar spinal cord. J Comp Neurol 388(4):565-574.

Bice TN, Beal JA. 1997. Quantitative and neurogenic analysis of the total population and subpopulations of neurons defined by axon projection in the superficial dorsal horn of the rat lumbar spinal cord. J Comp Neurol 388(4):550-564.

Braz JM, Basbaum AI. 2009. Triggering genetically-expressed transneuronal tracers by peripheral axotomy reveals convergent and segregated sensory neuron-spinal cord connectivity. Neuroscience 163:1220-1232.

Budd JM, Kovacs K, Ferecsko AS, Buzas P, Eysel UT, Kisvarday ZF. 2010. Neocortical axon arbors trade-off material and conduction delay conservation. PLoS Comput Biol 6(3):e1000711.

Cajal SRy. 1909. Histologie du systéme nerveux. Paris: A. Maloine. 986 p.

Cervero F, Iggo A, Molony V. 1979. Ascending projections of nociceptor-driven Lamina I neurones in the cat. Exp Brain Res 35(1):135-149.

Cervero F, Tattersall JE. 1987. Somatic and visceral inputs to the thoracic spinal cord of the cat: marginal zone (lamina I) of the dorsal horn. J Physiol 388:383-395.

Cheunsuang O, Morris R. 2000. Spinal lamina I neurons that express neurokinin 1 receptors: morphological analysis. Neuroscience 97(2):335-345.

Christensen BN, Perl ER. 1970. Spinal neurons specifically excited by noxious or thermal stimuli: marginal zone of the dorsal horn. J Neurophysiol 33(2):293-307.

Chung K, Coggeshall RE. 1988. Propriospinal fibers in the white matter of the cat sacral spinal cord. J Comp Neurol 269(4):612-617.

Debanne D, Campanac E, Bialowas A, Carlier E, Alcaraz G. 2011. Axon physiology. Physiol Rev 91(2):555-602.

Debanne D, Guerineau NC, Gahwiler BH, Thompson SM. 1997. Action-potential propagation gated by an axonal I(A)-like K+ conductance in hippocampus. Nature 389(6648):286-289.

Dickenson AH, Chapman V, Green GM. 1997. The pharmacology of excitatory and inhibitory amino acid-mediated events in the transmission and modulation of pain in the spinal cord. Gen Pharmacol 28(5):633-638.

Duflocq A, Chareyre F, Giovannini M, Couraud F, Davenne M. 2011. Characterization of the axon initial segment (AIS) of motor neurons and identification of a para-AIS and a juxtapara-AIS, organized by protein 4.1B. BMC Biol 9:66.

Eckert WA 3rd, McNaughton KK, Light AR. 2003. Morphology aand axonal arborization of rat spinal inner lamina II neurons hyperpolarized by mu-opioid-selective agonists. J Comp Neurol 458:240-256.

Ferrini F, Salio C, Vergnano AM, Merighi A. 2007. Vanilloid receptor-1 (TRPV1)-dependent activation of inhibitory neurotransmission in spinal substantia gelatinosa neurons of mouse. Pain 129(1-2):195-209.

Fleidervish IA, Lasser-Ross N, Gutnick MJ, Ross WN. 2010. Na+ imaging reveals little difference in action potential-evoked Na+ influx between axon and soma. Nat Neurosci 13(7):852-860.

Foust A, Popovic M, Zecevic D, McCormick DA. 2010. Action potentials initiate in the axon initial segment and propagate through axon collaterals reliably in cerebellar Purkinje neurons. J Neurosci 30(20):6891-6902.

Gobel S. 1978. Golgi studies of the neurons in layer I of the dorsal horn of the medulla (trigeminal nucleus caudalis). J Comp Neurol 180:375-394.

Grudt TJ, Perl ER. 2002. Correlations between neuronal morphology and electrophysiological features in the rodent superficial dorsal horn. J Physiol 540(Pt 1):189-207.

Guo C, Stella SL Jr., Hirano AA, Brecha NC. 2009. Plasmalemmal and vesicular gamma-aminobutyric acid transporter expression in the developing mouse retina. J Comp Neurol 512:6-26.

Hunt SP, Kelly JS, Emson PC, Kimmel JR, Miller RJ, Wu JY. 1981. An immunohistochemical study of neuronal populations containing neuropeptides or gamma-aminobutyrate within the superficial layers of the rat dorsal horn. Neuroscience 6(10):1883-1898.

Hylden JL, Hayashi H, Bennett GJ. 1986. Lamina I spinomesencephalic neurons in the cat ascend via the dorsolateral funiculi. Somatosens Res 4(1):31-41.

Jinno S, Klausberger T, Marton LF, Dalezios Y, Roberts JD, Fuentealba P, Bushong EA, Henze D, Buzsaki G, Somogyi P. 2007. Neuronal diversity in GABAergic long-range projections from the hippocampus. J Neurosci 27(33):8790-8804.

Lenhossék Mv. 1895. Der feinere Bau des Nervensystems im Lichte neuester Forschungen. Eine allgemeine Betrachtung der Strukturprincipien des Nervensystems, nebst einer Darstellung des feineren Baues des Rückenmarkes. Berlin: Kornfeld. 409 p.

Li J, Baccei ML. 2011. Pacemaker neurons within newborn spinal pain circuits. J Neurosci 31(24):9010-9022.

Li YQ, Li H, Yang K, Kaneko T, Mizuno N. 2000. Morphologic features and electrical membrane properties of projection neurons in the marginal layer of the medullary dorsal horn of the rat. J Comp Neurol 424(1):24-36.

Light AR, Trevino DL, Perl ER. 1979. Morphological features of functionally defined neurons in the marginal zone and substantia gelatinosa of the spinal dorsal horn. J Comp Neurol 186(2):151-171.

Lima D. 1998. Anatomical basis for the dynamic processing of nociceptive input. Eur J Pain 2(3):195-202.

Lima D, Coimbra A. 1986. A Golgi study of the neuronal population of the marginal zone (lamina I) of the rat spinal cord. J Comp Neurol 244(1):53-71.

Littlewood NK, Todd AJ, Spike RC, Watt C, Shehab SA. 1995. The types of neuron in spinal dorsal horn which possess neurokinin-1 receptors. Neuroscience 66(3):597-608.

Luz LL, Szucs P, Pinho R, Safronov BV. 2010. Monosynaptic excitatory inputs to spinal lamina I anterolateral-tract-projecting neurons from neighbouring lamina I neurons. J Physiol 588(Pt 22):4489-4505.

Manor Y, Koch C, Segev I. 1991. Effect of geometrical irregularities on propagation delay in axonal trees. Biophys J 60(6):1424-1437.

Mesnage B, Gaillard S, Godin AG, Rodeau JL, Hammer M, Von Engelhardt J, Wiseman PW, De Koninck Y, Schlichter R, Cordero-Erausquin M. 2011. Morphological and functional characterization of cholinergic interneurons in the dorsal horn of the mouse spinal cord. J Comp Neurol 519(16):3139-3158.

Millan MJ. 2002. Descending control of pain. Prog Neurobiol 66(6):355-474.

Morgan CW. 2001. Axons of sacral preganglionic neurons in the cat: I. Origin, initial segment, and myelination. J Neurocytol 30(6):523-544.

Paxinos G, Watson C. 2007. The rat brain in stereotaxic coordinates, 6th ed. New York: Academic Press.

Pinto V, Derkach VA, Safronov BV. 2008. Role of TTX-sensitive and TTX-resistant sodium channels in Adelta- and C-fiber conduction and synaptic transmission. J Neurophysiol 99(2):617-628.

Pinto V, Szucs P, Lima D, Safronov BV. 2010. Multisegmental A{delta}- and C-fiber input to neurons in lamina I and the lateral spinal nucleus. J Neurosci 30(6):2384-2395.

Polgar E, Hughes DI, Riddell JS, Maxwell DJ, Puskar Z, Todd AJ. 2003. Selective loss of spinal GABAergic or glycinergic neurons is not necessary for development of thermal hyperalgesia in the chronic constriction injury model of neuropathic pain. Pain 104(1-2):229-239.

Polgar E, Sardella TCP, Watanabe M, Todd AJ. 2011. A quantitative study of NPY-expressing GABAergic neurons and axons in rat spinal dorsal horn. J Comp Neurol 519:1007-1023.

Safronov BV. 1999. Spatial distribution of NA+ and K+ channels in spinal dorsal horn neurones: role of the soma, axon and dendrites in spike generation. Prog Neurobiol 59(3):217-241.

Safronov BV, Pinto V, Derkach VA. 2007. High-resolution single-cell imaging for functional studies in the whole brain and spinal cord and thick tissue blocks using light-emitting diode illumination. J Neurosci Methods 164(2):292-298.

Safronov BV, Wolff M, Vogel W. 1997. Functional distribution of three types of Na+ channel on soma and processes of dorsal horn neurones of rat spinal cord. J Physiol 503 (Pt 2):371-385.

Schoenen J. 1982. The dendritic organization of the human spinal cord: the dorsal horn. Neuroscience 7(9):2057-2087.

Spike RC, Puskar Z, Andrew D, Todd AJ. 2003. A quantitative and morphological study of projection neurons in lamina I of the rat lumbar spinal cord. Eur J Neurosci 18(9):2433-2448.

Szentagothai J. 1964. Neuronal and Synaptic Arrangement in the Substantia Gelatinosa Rolandi. J Comp Neurol 122:219-239.

Szucs P, Luz LL, Lima D, Safronov BV. 2010. Local axon collaterals of lamina I projection neurons in the spinal cord of young rats. J Comp Neurol 518(14):2645-2665.

Szucs P, Pinto V, Safronov BV. 2009. Advanced technique of infrared LED imaging of unstained cells and intracellular structures in isolated spinal cord, brainstem, ganglia and cerebellum. J Neurosci Methods 177(2):369-380.

Todd AJ. 2010. Neuronal circuitry for pain processing in the dorsal horn. Nat Rev Neurosci 11(12):823-836.

Todd AJ, McGill MM, Shehab SA. 2000. Neurokinin 1 receptor expression by neurons in laminae I, III and IV of the rat spinal dorsal horn that project to the brainstem. Eur J Neurosci 12(2):689-700.

Todd AJ, Hughes DI, Polgar E, Nagy GG, Mackie M, Ottersen OP, Maxwell DJ. 2003. The expression of vesicular glutamate transporters VGLUT1 and VGLUT2 in neurochemically defined axonal populations in the rat spinal cord with emphasis on the dorsal horn. Eur J Neurosci 17(1):13-27.

Wang D, Li YQ, Li JL, Kaneko T, Nomura S, Mizuno N. 2000. gamma-aminobutyric acid- and glycine-immunoreactive neurons postsynaptic to substance P-immunoreactive axon terminals in the superficial layers of the rat medullary dorsal horn. Neurosci Lett 288(3):187-190.

Westrum LE, Blackstad TW. 1962. An electron microscopic study of the stratum radiatum of the rat hippocampus (regio superior, CA 1) with particular emphasis on synaptology. J Comp Neurol 119:281-309.

Willis WD, Coggeshall RE. 1991. Sensory Mechanisms of the Spinal Cord. New York: John Wiley.

Yasaka T, Tiong SY, Hughes DI, Riddell JS, Todd AJ. 2010. Populations of inhibitory and excitatory interneurons in lamina II of the adult rat spinal dorsal horn revealed by a combined electrophysiological and anatomical approach. Pain 151(2):475-488.

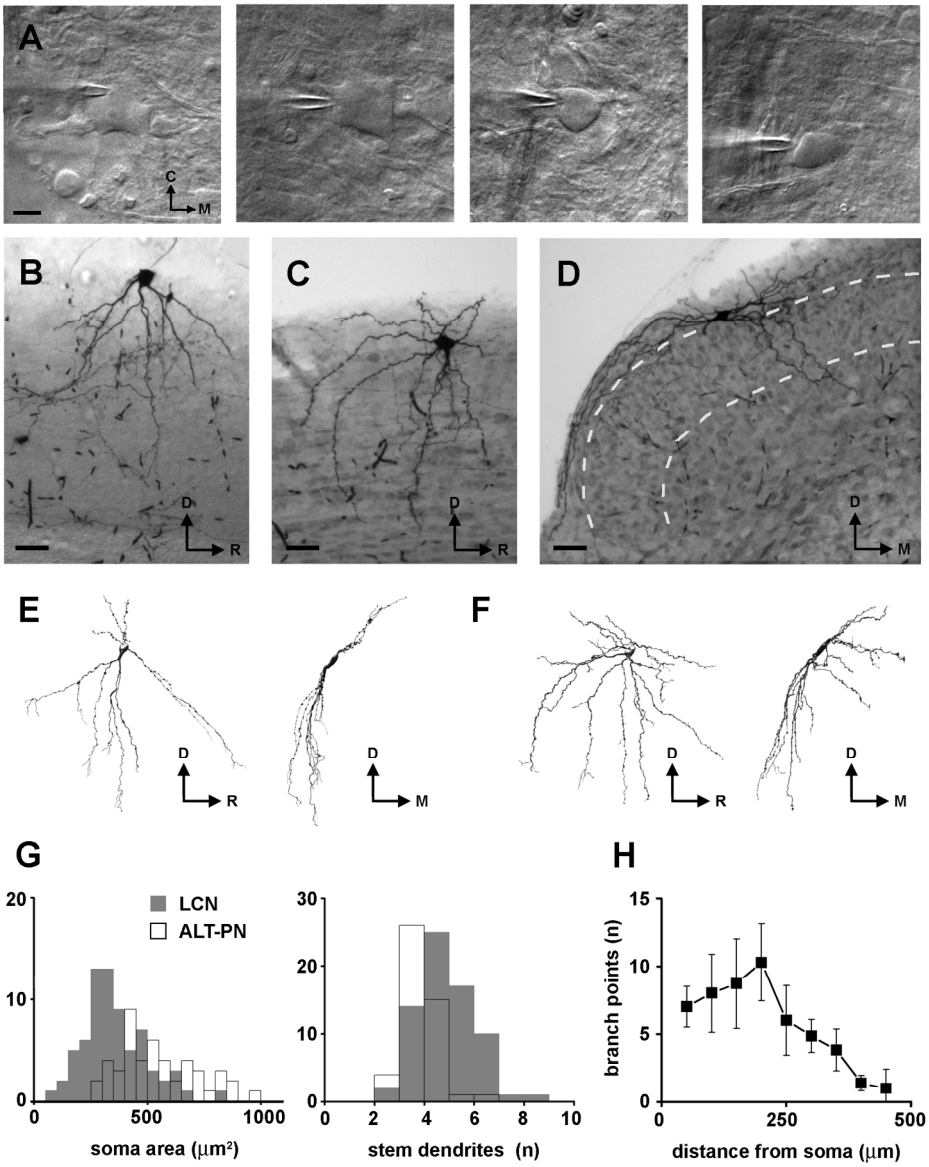

Figure 1. Somatodendritic features of LCNs. **A:** Images of large (left pair) and smaller (right pair) LCNs during the process of cell labeling. **B:** Photomicrograph of the soma, dendrites and axon branches of a typical flattened LCN in a sagittal spinal cord section. **C:** Photomicrograph of a typical multipolar LCN in a sagittal section. **D:** Another multipolar LCN in a transverse section. Dashed white line indicates the rough borders of lamina II. The section is slightly distorted due to detachment from the supporting agar during processing. **E:** Sagittal (left) and transverse (right) rotated views of a 3-D reconstructed flattened LCN (reconstruction from sagittal sections; axon omitted for clarity). **F:** Sagittal (left) and transverse (right) rotated views of a 3-D reconstructed multipolar LCN (reconstruction from sagittal sections; axon omitted for clarity). **G:** Histograms of soma area distribution (left) and number of stem dendrites (right) in LCNs (gray bars) and ALT-PNs (outlined empty bars). The data for the ALT-PNs are from Szucs et al. (2010). **H:** 3-D Sholl analysis of the number of dendritic branch points in 50-µm-thick shells. C, caudal; M, medial; D, dorsal; R, rostral (throughout the figures). Binsizes in G = 50 μm^2 in the soma area histogram; 1 in the stem dendrite histogram. Scale bars = 20 µm in A; 50 µm in B-D.

219x279mm (300 x 300 DPI)

Figure 2. A typical multipolar LCN reconstructed from transverse serial sections. **A:** Overlaid image of 15 transverse, 100 µm thick, serial sections. Dendrites (black) and axon (dark gray) of the LCN (cell ID: L316_E6) occupy laminae I-II and protrude into lamina III. An axon collateral descends ventrally beyond the neck of the dorsal horn, while some dendrites are located in the DLF. For clarity, borders of the white and gray matter (continuous light gray line; same in B and C) as well as of lamina II (dashed light gray line; same in B and C) are only shown for the section containing the cell body. **B:** Reconstructions showing the location of dendritic pieces (black) in the individual transverse serial sections. **C:** Reconstructions indicating the location of axonal pieces (black) in the individual transverse serial sections. soma, section with the cell body; r, rostral; c, caudal. Scale bar = 500 µm.
229x637mm (300 x 300 DPI)

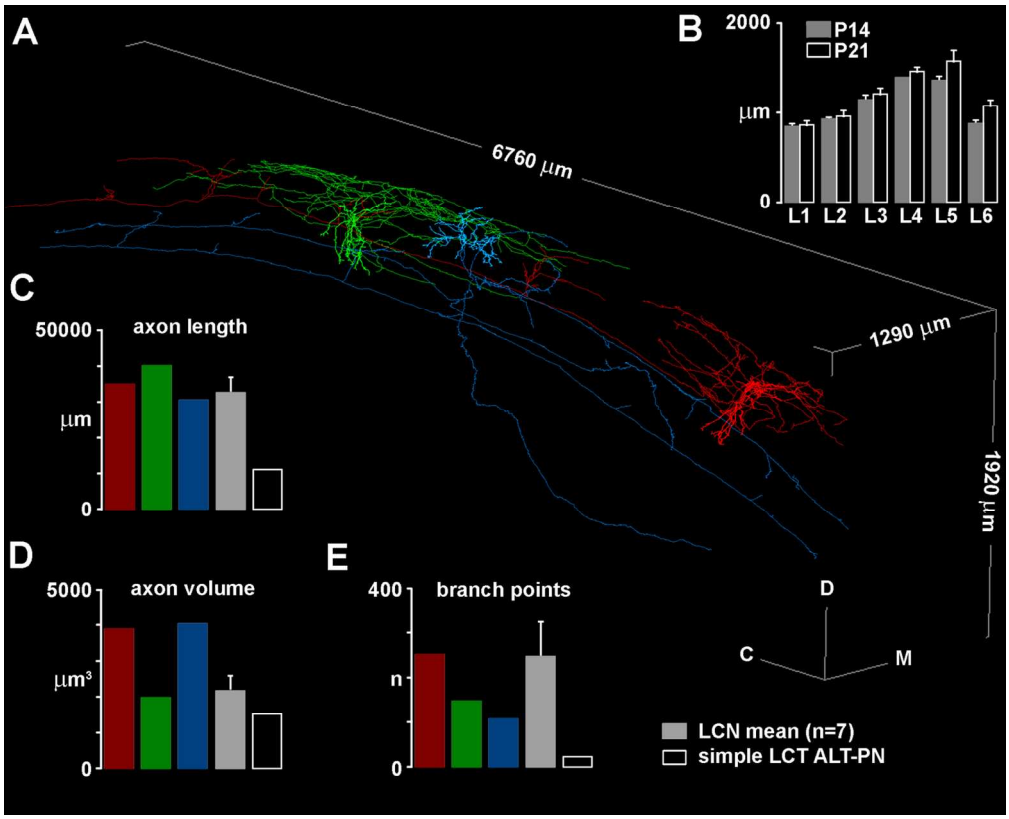

Figure 3. Comparison of basic axon parameters of 3-D reconstructed LCNs and ALT-PNs. **A:** 3-D reconstruction of two LCNs (cell ID: L292_E1 - in red; cell ID: L292_E5 - in green) and a mixed-collateral-type (MCT) ALT-PN (cell ID: L292_E4 - in blue), filled in the same spinal cord. Rostrocaudal, mediolateral and dorsoventral dimensions of the bounding box (light gray) are indicated along the corresponding axis. **B:** Length of different lumbar spinal cord segments (L1-L6) at postnatal days 14 (P14) and 21 (P21). Columns in each case show the average and standard mean error of measurements in 3 different animals. **C-E:** Total axon length (i.e. sum of the lengths of all reconstructed axon segments), total axon volume (i.e. sum of all reconstructed axon segment volumes, calculated from segment length and local diameter) and number of branch points along the axon of individual cells (red, green, blue and white outline columns) along with the mean value for 3-D reconstructed LCNs (gray column; n = 7).
140x113mm (300 x 300 DPI)

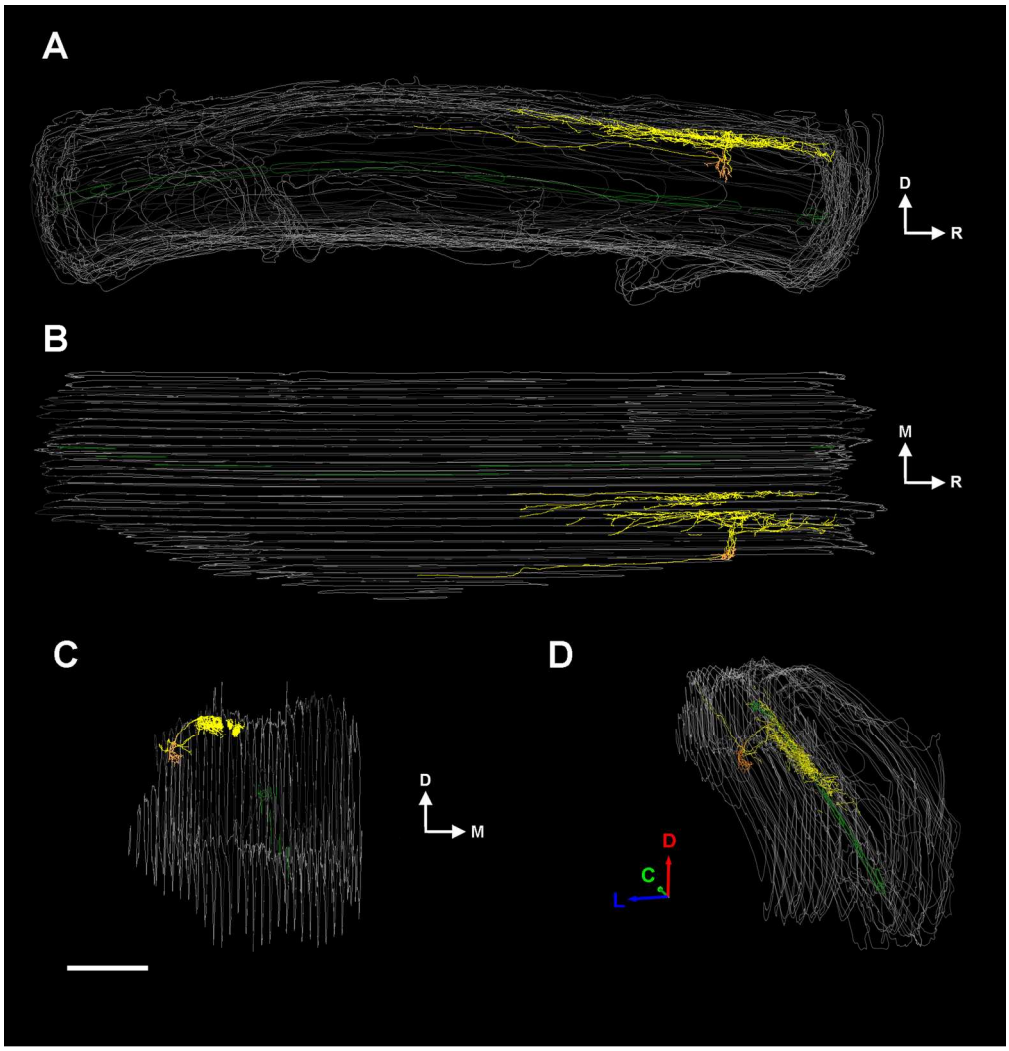

Figure 4. Sagittal (**A**), horizontal (**B**), transverse (**C**) and perspective (**D**) view of a 3-D reconstructed but not fully connected LCN (cell ID: Zs079_E13). The majority of the axon (yellow) in this case is located medially, considerably remote from the lateral cell body and dendrites (orange). The neuron has a solitary branch running caudally in the dorsolateral funiculus on the ipsilateral side. The medial part of the axonal tree, due to distortion of some sections, could not be connected to form a single axon. White and gray matter borders are indicated with gray and central canal is shown in green. Scale bar = 1 mm.
180x187mm (300 x 300 DPI)

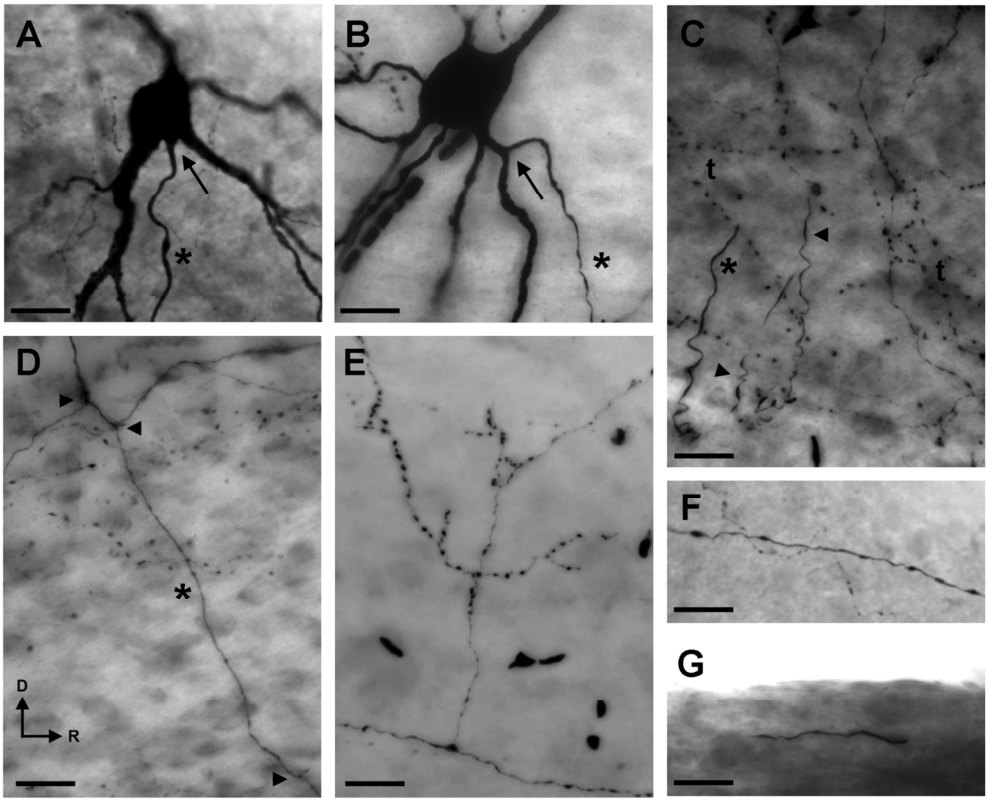

Figure 5. General morphological features of the axon of LCNs. Main axon (asterisk) originating from the soma (**A**) and from a primary dendrite (**B**) of two LCNs. Arrows point at the axon origin. **C:** Characteristic appearance of LCN axons in the vicinity of the cell body. The main axon (asterisk) along with primary and secondary order branches (arrowheads) are intermingled with fine terminal branches enriched with varicosities (t). **D:** The main axon (asterisk) of an LCN giving rise to primary branches (arrowheads) in an alternating manner. **E:** Perpendicular side branch from a solitary axon branch running in the dorsolateral funiculus. **F:** Straight thick solitary axon with swellings together with a more undulated thin varicose also solitary branch next to the surface of the preparation, most likely in the Lissauer tract. **G:** Thick, myelinated looking solitary branch of an LCN, running in the dorsal funiculus. A-E, G - extended focal images; F - single focal plane image. Scale bars = 25 μm.
139x113mm (300 x 300 DPI)

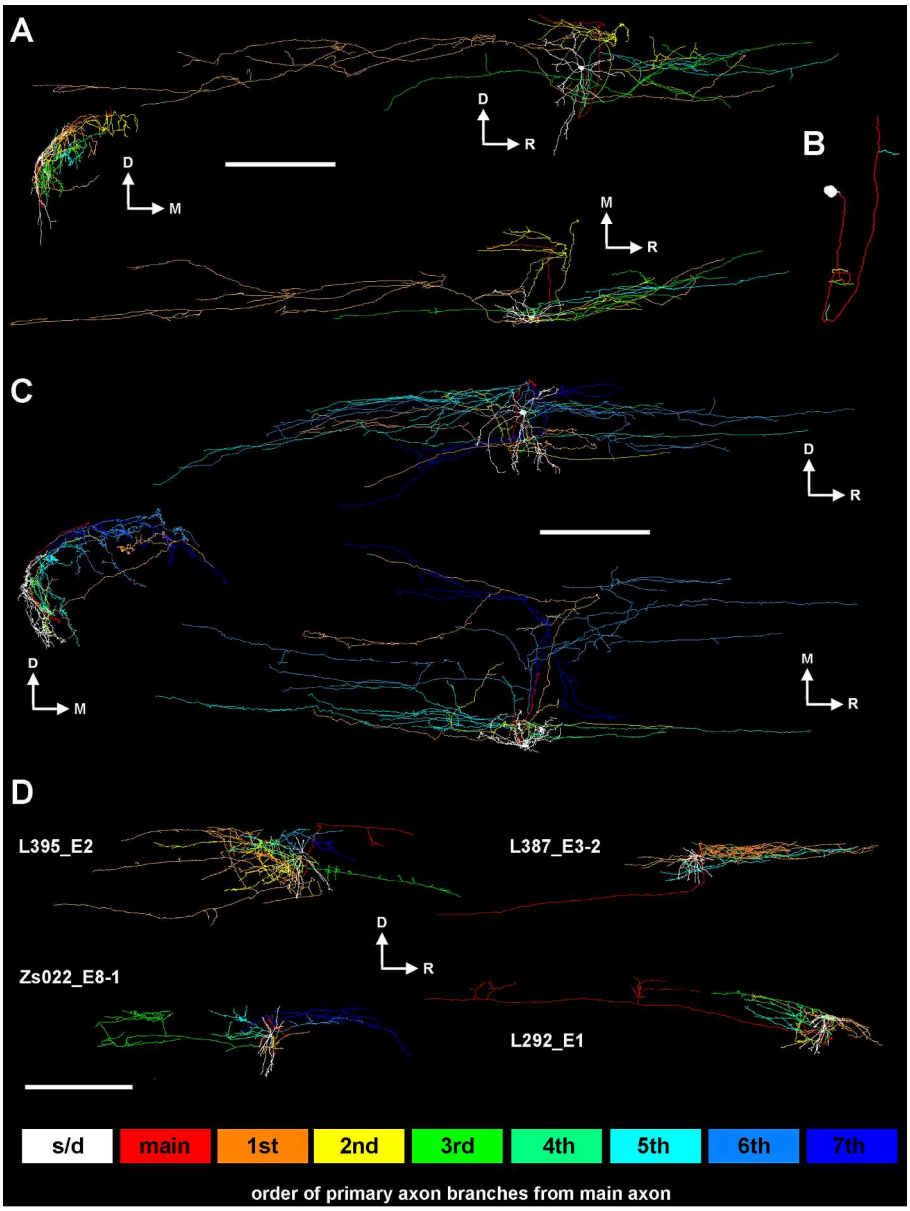

Figure 6. Organization of the primary axon branches of LCNs. **A:** Sagittal (top), transverse (middle left) and horizontal (bottom) view of the 3-D reconstruction of an LCN with 5 primary branches (cell ID: L420_E2) where the first and second branches (orange and yellow) dominate the tree showing partial overlap with the rest of the branches. The end of the main axon turns caudally and finishes abruptly close to the surface; most likely damaged when pia mater was removed during preparation. **B:** Main axon and the origination points of each primary branch. Note the dorsoventral loop of the main axon. **C:** Another LCN (cell ID: L292_E5) with 7 primary branches, from which the last two (light blue and dark blue) covers the largest area. Similarly to the previous cell, the main axon forms a loop before it finishes abruptly close to the surface with a visible swelling at the end, probably caused by truncation. The first primary branch (orange) of this axon traverses the dorsal horn medially and target similar regions than the last branch (dark blue). **D:** Sagittal view of 3-D reconstructions of 4 other LCNs. Cell IDs are indicated on the left side of the corresponding reconstruction. Colored boxes in the bottom of the figure indicate the color codes of the sequence of primary axon branches. S/d, soma and dendrites; main, main axon; 1st-7th, the respective

order of primary branches from the main axon. Scale bars = 500μm in A and C; 1 mm in D.
229x305mm (300 x 300 DPI)

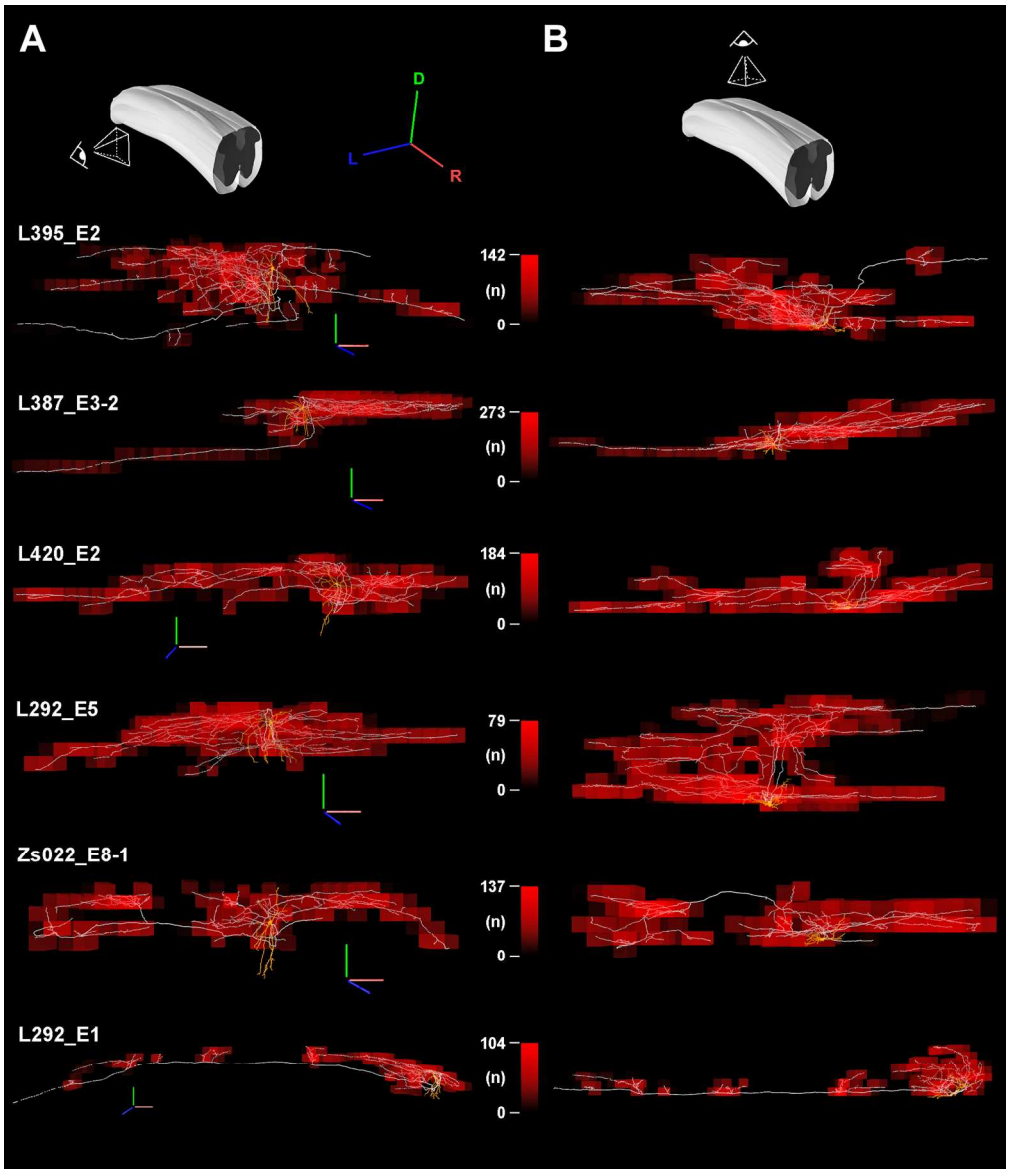

Figure 7. Varicosity distribution along the axon of LCNs. Spatially dependent visual representation of axon varicosity distribution from sagittal (**A**) and horizontal (**B**) views, as indicated on the schematic drawings above each column. Axon varicosities along the 3-D reconstructed LCN axons were counted in predetermined space units (voxel). The maximum varicosity number in the predefined voxels (100 µm x 100 µm x 100 µm) is indicated as the maximum value (red) on the scale bar next to the particular neuron. The actual number of varicosities in a voxel is used as a color and opacity value for the cube representing that voxel. Cell IDs are indicated on the left side of the figure. 3-D scale bars (D, dorsal - green; L, lateral - blue; R, rostral - red) = 250 µm.
200x233mm (300 x 300 DPI)

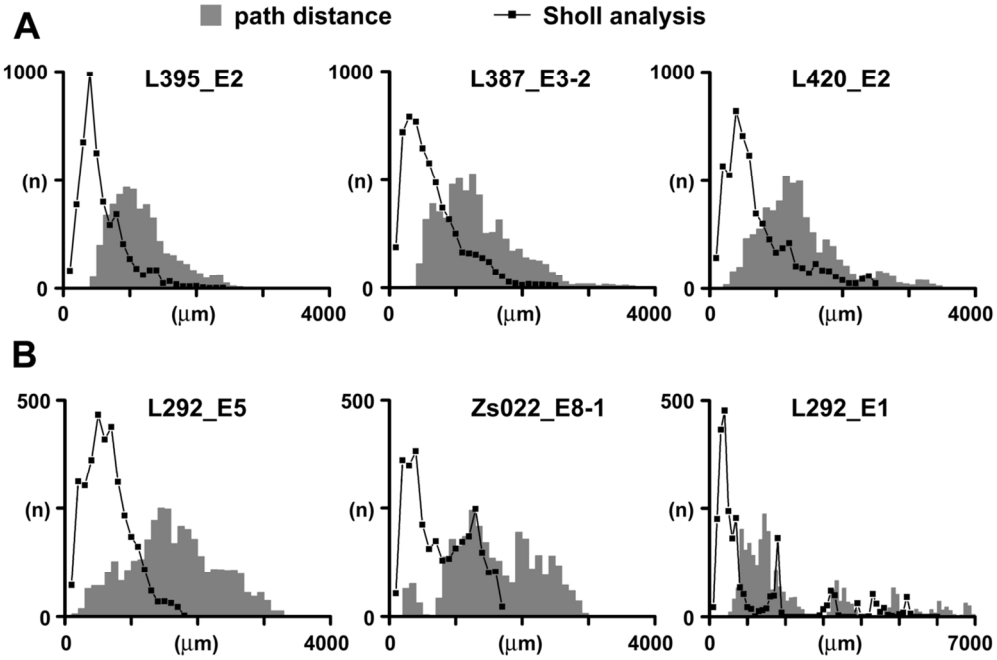

Figure 8. Physical and path distance of axon varicosities in 3-D reconstructed LCN axons. Sholl analysis was performed using 100 µm shells. Binsize in path distance histograms is 100 µm. **A:** Three cells showing a major accumulation of varicosities in the vicinity of, but not centered on the soma, with one peak both in the Sholl analysis and in the path distance histogram. **B:** Other LCNs, with lower overall number of varicosities, showed additional local accumulations, evidenced by multiple peaks in the Sholl analysis, and at the same time wider distribution of the path distance histogram. Notice the different scaling of the Y-axis between A and B and also the difference on the X-axis in cell ID: L292_E1 in part B.
119x83mm (300 x 300 DPI)

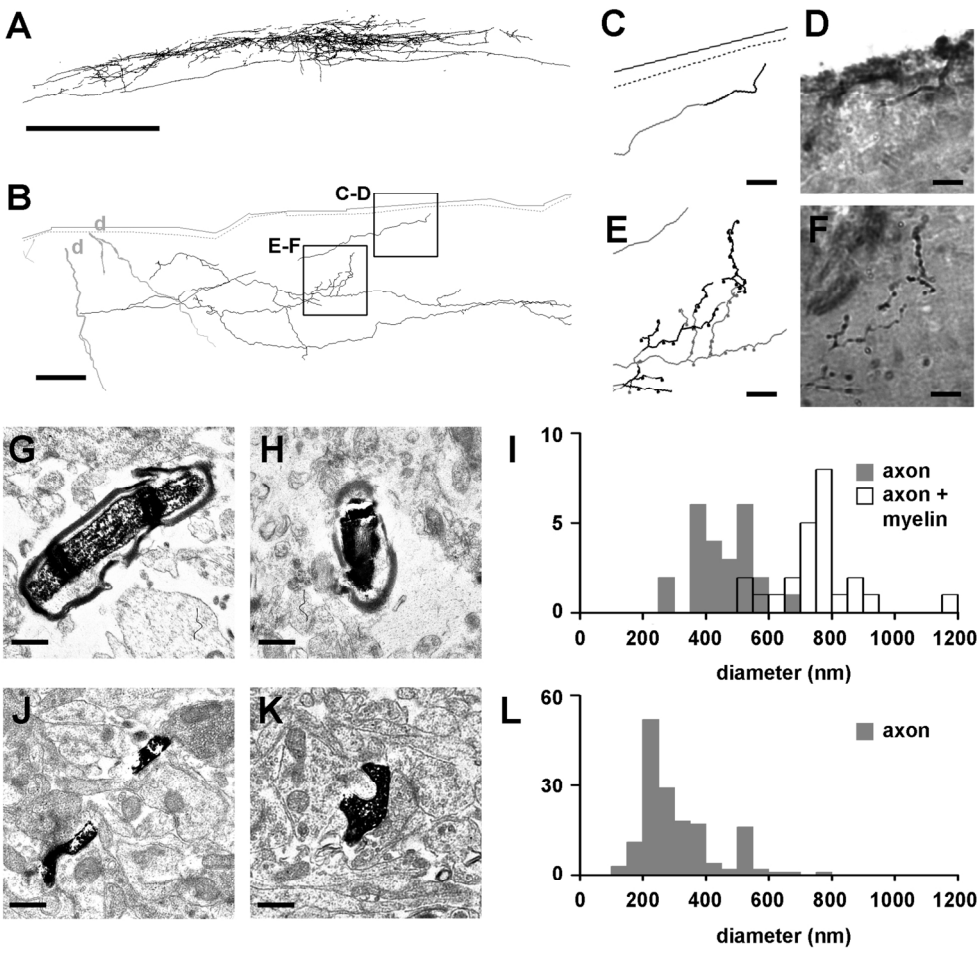

Figure 9. Fine structural difference between myelinated and unmyelinated parts of an LCN axon. **A:** 2-D reconstruction of a representative LCN axon (cell ID: L279_E2). **B:** 2-D reconstruction of a single section of the same axon. Light gray processes are dendrites (d) while axon is in black. Continuous and dotted gray lines indicate the border of the section and border between the gray- and white matter, respectively. Boxes indicate regions of interest with a single myelinated looking axon branch (C-D) and several varicose branches (E-F). **C-F:** show the reconstruction of the corresponding region and a photomicrograph of the same region from the surface of the block used for preparing the electron microscopy sections. Black parts of the reconstructions in C and E show axon pieces still present on the block surface, while gray indicate parts that were already cut. **G-H:** Electron microscopic images of axon profiles from region C-D with several concentric layers of myelin. **I:** Diameter histogram of axon profiles (n = 24) from the same region measured with (outlined hollow bars) and without myelin (gray bars). **J:** Electron microscopic image of an inter-varicosity segment and a varicosity (**K**) from region E-F. **L:** Diameter histogram of axon profiles (n = 157) from the same region. Bins = 50 nm in I and L. Scale bars = 1 mm in A; 50 µm in B; 10 µm in C, D, E and F; 500 nm in G, H, J and K.
170x167mm (300 x 300 DPI)

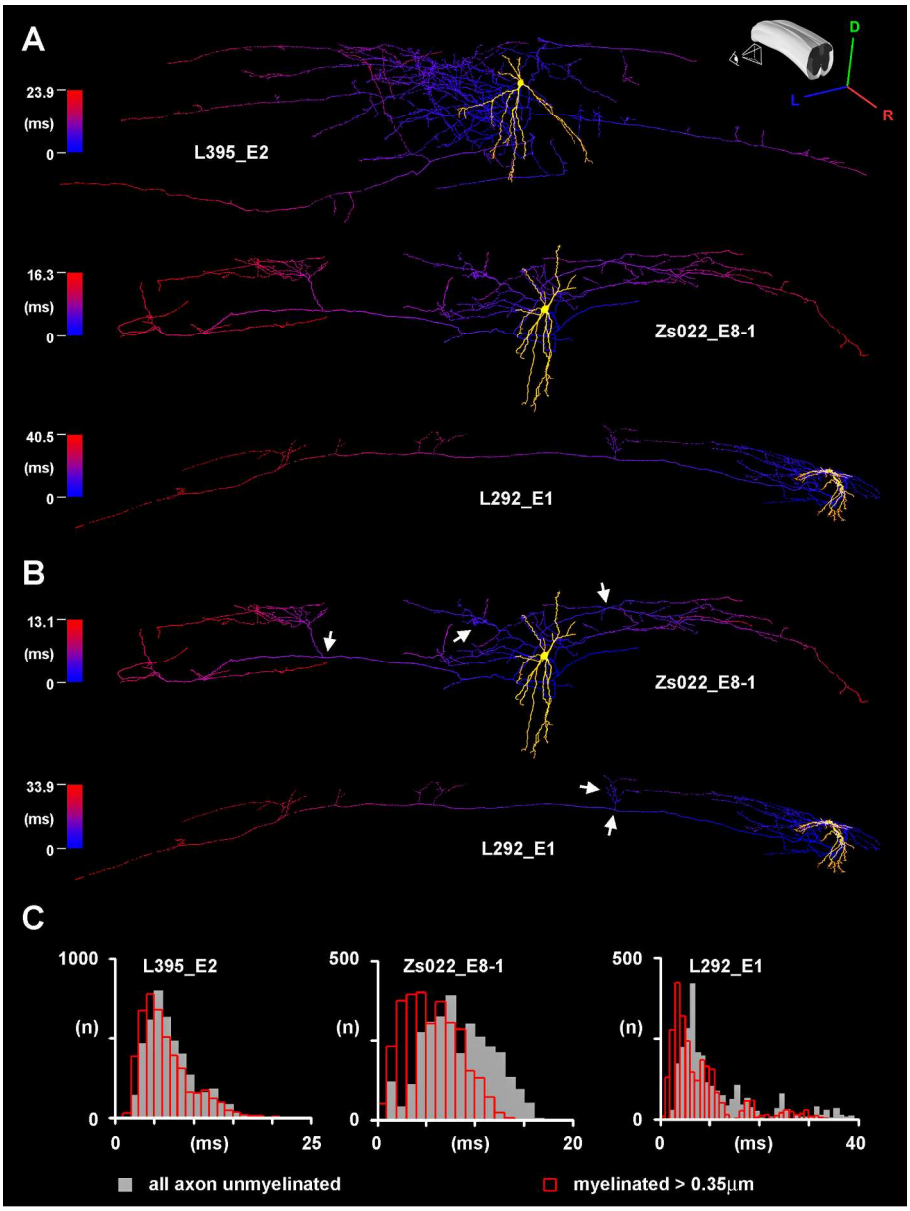

Figure 10. Action potential propagation time maps of LCN axons. **A:** Sagittal view (see schematic figure in upper right) of a cell (ID: L395_E2) with a more compact tree and two cells (IDs: Zs022_E8-1 and L292_E1) with distant terminal branching areas. The whole axon is considered unmyelinated. **B:** AP propagation time maps of two cells (IDs: Zs022_E8-1 and L292_E1) re-plotted assuming that axon pieces with a diameter above 0.35 µm are myelinated. The maximum propagation time value in the map is indicated by red, while 0 ms is blue on the scale bar next to the particular neuron. Arrows point at regions where the propagation time map shows visible differences. **C:** Propagation time histogram of the axon varicosities of the three LCNs shown in A. Bins = 1 ms. Gray bars, total axon unmyelinated; red outlined transparent bars, axon pieces with a diameter above 0.35 µm are myelinated.
229x305mm (300 x 300 DPI)

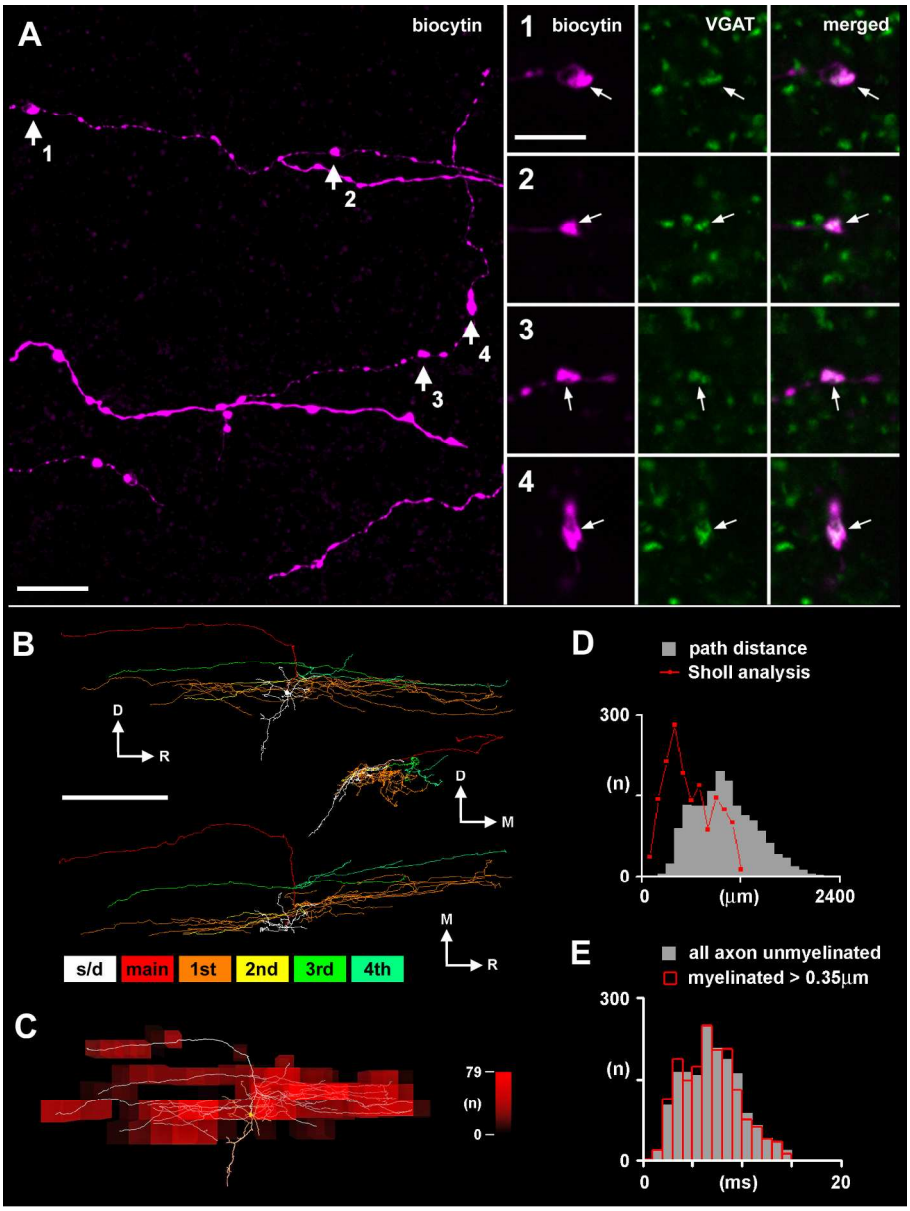

Figure 11. Example of an inhibitory LCN. **A:** Single section of a biocytin filled axon (magenta) of an LCN (cell ID: L571_E20-3). Arrows with numbers indicate the VGAT immunoreactive axon varicosities (green) shown in detail in the insets on the right side. Small arrows in the inset point at the actual varicosity. The main image is projected from 36 optical sections at 0.5 µm z-spacing, while images in the insets are single optical sections. **B:** Primary branch organization of the same LCN axon shows relatively few overlap between the branches. **C-D:** The number of axon varicosities in this axon is moderate and varicosity distribution show more than one, relatively dispersed accumulations. **E:** Temporal dispersion of action potential propagation times in the same LCN axon did not show noticeable difference when using the diameter threshold for myelinated axons, indicating the lack of long myelinated parts in the axon. Scale bars = 10 µm in A; 5 µm in insets. Bins = 100 µm in D; 1 ms in E.
229x305mm (300 x 300 DPI)

TABLE 1.
Details of the Antibodies Used

Antibody	Host	Antigen	Amino acid sequence	Supplier	Catalogue number	Dilution
VGLUT2	Guinea pig	18 amino acids at C-terminal end of rat VGLUT2	VQESAQDAYSYKDRDDYS	Millipore	AB2251	1:5.000
VGAT	Rabbit polyclonal	amino acids 75-87 of rat VGAT coupled to KLH	AEPPVEGDIHYQR	Synaptic Systems	131 002	1:1.000

TABLE 2.
Basic Morphometric Parameters of the Somatodendritic and Axonal Domain of LCNs[1]

		soma		dendritic tree dimensions			axonal tree dimensions				plane	
SD type	n	area (μm^2)	stem	RC (μm)	ML (μm)	DV (μm)	RC (μm)	ML (μm)	DV (μm)	cut	S	T
flattened	29	357 ± 30 (93 - 679)	4.2 ± 0.2 (3 - 6)	301 ± 21 (150 - 500)	304 ± 19 (200 - 620)	65 ± 25 (25 - 110)	2429 ± 205 (800 - 5200)	656 ± 43 (400 - 1100)	288 ± 40 (124 - 479)	18	23	6
multipolar	38	357 ± 23 (110 - 839)	4.8 ± 0.2 (2 - 8)	323 ± 17 (140 - 500)	327 ± 21 (197 - 634)	178 ± 16 (107 - 250)	2401 ± 173 (1100 - 6500)	691 ± 41 (312 - 1300)	331 ± 84 (133 - 1050)	22	30	8
other + n.c.	5	261 ± 30 (172 - 304)	3.0 ± 0.4 (2 - 4)	437 ± 134 (260 - 700)	405 ± 105 (300 - 720)	260	1868 ± 145 (700 - 2700)	459 ± 38 (240 - 800)	248 ± 67 (120 - 680)	11	7	8
no soma recovered	10	n.a.	n.a.	n.a.	n.a.	n.a.						
all LCNs [2]	82	351 ± 17 (93 - 839)	4.4 ± 0.1 (2 - 8)	320 ± 14 (140 - 700)	323 ± 15 (197 - 720)	159 ± 19 (25 - 260)	2312 ± 113 (700 - 6500)	636 ± 27 (240 - 1300)	295 ± 41 (120 - 1050)	51	60	22

TABLE 3.
Morphological Description of the Axon of LCNs[1]

		axon origin		location of axon branches				
SD type	n	dendrite	distance (µm)	only local within GM	neighboring WM (thin with varicosities)	Lissauer / DF (thick, no varicosities)	DLF / LF (thick, no varicosities)	ipsi- or contra-ALT
flattened	29	17 (59 %)	22 ± 3 (3 - 60)	4 (14 %)	12 (41 %)	9 (31 %)	4 (14 %)	0 (0 %)
multipolar	38	26 (68 %)	12 ± 1 (4 - 26)	12 (31 %)	14 (37 %)	9 (24 %)	3 (8 %)	0 (0 %)
other + n.c.	5	3 (60 %)	16 ± 5 (8 - 28)	7 (46 %)	6 (40 %)	1 (7 %)	1 (7 %)	0 (0 %)
no soma recovered	10	n.a.	n.a.					
all LCNs[2]	82	46 (64 %)	16 ± 2 (3 - 60)	23 (28%)	32 (39 %)	19 (23 %)	8 (10 %)	0 (0 %)

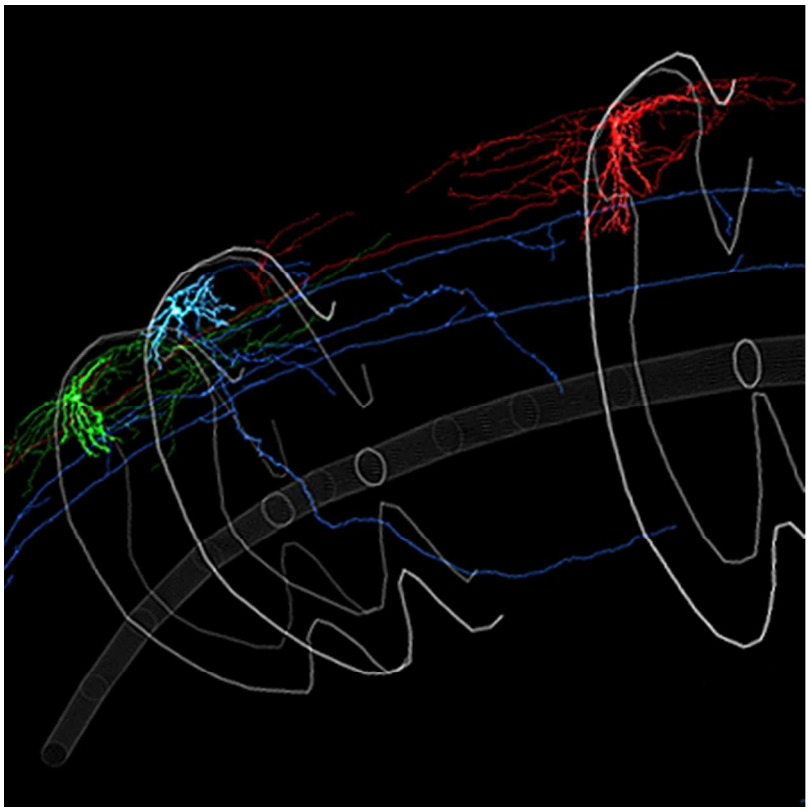

Using an intact spinal cord preparation the authors describe axon architecture of lamina I local circuit neurons (red and green). Extensive local- and long rostrocaudal axon branches suggest information feed towards deeper laminae as well as neighboring segments, providing anatomical substrate for interlaminar and intersegmental processing in the dorsal horn.
141x141mm (72 x 72 DPI)

Using an intact spinal cord preparation the authors describe axon architecture of lamina I local circuit neurons (red and green). Extensive local- and long rostrocaudal axon branches suggest information feed towards deeper laminae as well as neighboring segments, providing anatomical substrate for interlaminar and intersegmental processing in the dorsal horn.